

**UNIVERSITY OF SÃO PAULO  
CENTER FOR NUCLEAR ENERGY IN AGRICULTURE**

**Analysis of hydraulic properties and 3D images of some tropical soils**

**LÍVIA PREVIA TELLO DA SILVA**

**Piracicaba**

**2017**



**LÍVIA PREVIATELLO DA SILVA**

**Analysis of hydraulic properties and 3D images of some tropical soils**

**Thesis presented for the degree of Doctor of  
Science at the Center for Nuclear Energy in  
Agriculture of the University of São Paulo**

**Concentration Area: Nuclear Energy in  
Agriculture and Environment**

**Supervisor: Prof. Dr. Quirijn de Jong van Lier**

**Piracicaba**

**2017**

AUTORIZO A DIVULGAÇÃO TOTAL OU PARCIAL DESTE TRABALHO, POR QUALQUER MEIO CONVENCIONAL OU ELETRÔNICO, PARA FINS DE ESTUDO E PESQUISA, DESDE QUE CITADA A FONTE.

Dados Internacionais de Catalogação na Publicação (CIP)

**Seção Técnica de Biblioteca - CENA/USP**

Silva, Livia Previatello da

Análise das propriedades hidráulicas e imagens 3D de alguns solos tropicais / Analysis of hydraulic properties and 3D images of some tropical soils / Livia Previatello da Silva; orientador Quirijn de Jong van Lier. - - Piracicaba, 2017.

72 p. : il.

Tese (Doutorado – Programa de Pós-Graduação em Ciências. Área de Concentração: Energia Nuclear na Agricultura e no Ambiente) – Centro de Energia Nuclear na Agricultura da Universidade de São Paulo.

1. Água do solo 2. Condutividade hidráulica do solo 3. Evaporação 4. Imagem 3D 5. Microtomografia 6. Solo tropical I. Título

CDU 631.434 + 631.445.7

Dedicated to

My parents, Jorge Luiz Bezerra da Silva and Márcia Previatello da Silva, for the support, understanding and love;

My sisters, Ana Carolina Previatello da Silva, Marília Previatello da Silva and my brother, Vinícius Previatello da Silva (*in memoriam*);

My family, especially my grandmother Gilda Borim, and my friends, for the understanding of distance and absence.



## ACKNOWLEDGMENTS

To my Family and my friends.

To professor Dr. Quirijn de Jong van Lier.

To the Centro de Energia Nuclear na Agricultura at the Universidade de São Paulo.

To FAPESP (São Paulo Research Foundation) for granting a national scholarship (2013/14669-0) for the development of the thesis and an international scholarship for the funding of my internship abroad (2014/05930-9).

To professors Sergio Oliveira Moraes, Paulo Leonel Libardi, Fábio Marin, Felipe Pilau, Paulo Sentelhas and Miguel Cooper for their teaching, and especially to my undergraduate advisor Marcus Metri Correa (UFRPE) for the constant encouragement during my research initiation.

To the technicians from the Soil Physics Lab at Cena, Robson and João Eduardo.

To the employees of the Technical Section of Informatics and Academic Directorate at Cena.

To my friends that I made in Piracicaba over the years, in special, Conan Ayade Salvador, Bruna Botin Nascimento, Jefferson Vieira José and Rafaelly Suzanye da Silva Santos.

To my friends from Fisol and Esalq, Everton Alves, Verena Benício, Victor Meriguetti, André Herman, Marcos Alex, Ana Paula Schwantes, Thaís Tavares, Yeleine Almoza, Leonardo Inforsato and Ali Mehmandoost.

To Katharina Meurer, Alena Roos, Steffen Schlüter, John Maximilian Köhne, and, in special to Hans-Jörg Vogel, for receiving me at UFZ and offering me all the help I needed.



“Words have a magical power. They can bring either the greatest happiness or deepest despair; they can transfer knowledge from teacher to student; words enable the orator to sway his audience and dictate its decisions. Words are capable of arousing the strongest emotions and prompting all men's actions”.

(Sigmund Freud)



## ABSTRACT

SILVA, L. P. da. **Analysis of hydraulic properties and 3D images of some tropical soils.** 2017. 72 p. Tese (Doutorado) – Centro de Energia Nuclear na Agricultura, Universidade de São Paulo, Piracicaba, 2017.

Mass and energy flow processes in soil are strongly dependent on the state of the soil structure and on pore space geometry. To correctly describe these transport processes, an adequate pore space characterization is required. In this context, the use of computerized microtomography allows the visualization of the soil structures and processes that occur at large scales may be very useful, besides being a fast and non-destructive technique. Soil hydraulic properties, which are essential in the quantification of water balance components in hydrological models of the unsaturated zone, can be measured directly with field or laboratory methods. Simultaneous determination of these properties can be done by the Wind-Schindler evaporation method, but determining only the retention function is a more common practice. The relation between soil water retention and hydraulic conductivity can then be predicted using theories like those developed by Childs and Collis-George, Burdine and Mualem. These models treat pore-space tortuosity and connectivity as an empirical parameter, and its value remains usually undetermined, the use of a standard value being more common. Based on this contextualization, the objectives of this thesis are: (i) to evaluate the correlation between soil hydraulic properties measured in the laboratory, and parameters that quantify soil pore space from 3D images obtained by X-ray microtomography; and (ii) to functionally analyze soil hydraulic property parameterization in the prediction of soil water balance components by an agrohydrological model. To verify the relationship between soil hydraulic properties and soil image parameters, a stepwise multiple regression analysis was performed between the pore space parameters from images and empirical parameters of the semi-deterministic model, obtained with evaporation experiments together with an inverse solution method. Functional evaluation of soil hydraulic parameters was performed by a sensitivity analysis of the outputs of an agro-hydrological model to several ways of obtaining the tortuosity/connectivity parameter: applying the commonly used standard value, or determining its value in evaporation experiments in the laboratory with wet-range tensiometers, dry-range tensiometers, or both wet- and dry-range tensiometers. Simulations with the agro-hydrological model were performed for some years with distinct rainfall characteristics. The soil retention curve obtained using soil images had a good

agreement to the retention curve obtained by the evaporation experiment, although the spatial resolution of the microtomograph allowed to only quantify macropores, consequently, to determine the hydraulic properties in a small range close to saturation. Soil hydraulic parameterization using a wide range of pressure heads is recommended for a better representation of vadose zone processes and soil-water-plant relations.

**Keywords:** Soil hydraulic properties. Evaporation experiment. Microtomography. 3D soil images.

## RESUMO

SILVA, L. P. da. **Análise das propriedades hidráulicas e imagens 3D de alguns solos tropicais.** 2017. 72 p. Tese (Doutorado) – Centro de Energia Nuclear na Agricultura, Universidade de São Paulo, Piracicaba, 2017.

Os processos de fluxo de massa e energia no solo dependem fortemente do estado da estrutura do solo e da geometria do espaço dos poros. Para descrever corretamente esses processos de transporte, é necessária uma caracterização adequada do espaço poroso. Neste contexto, o uso da microtomografia computadorizada permite a visualização das estruturas do solo e os processos que ocorrem em grandes escalas podem ser muito úteis, além de ser uma técnica rápida e não destrutiva. As propriedades hidráulicas do solo, que são essenciais na quantificação dos componentes do balanço hídrico em modelos hidrológicos da zona não saturada, podem ser medidas diretamente com métodos de campo ou laboratório. A determinação simultânea dessas propriedades pode ser feita pelo método de evaporação Wind-Schindler, mas a determinação apenas da função de retenção é uma prática mais comum. A relação entre a retenção de água do solo e a condutividade hidráulica pode então ser predita por teorias como as desenvolvidas por Childs e Collis-George, Burdine e Mualem. Esses modelos tratam a tortuosidade e conectividade do espaço poroso como um parâmetro empírico, e seu valor permanece geralmente indeterminado, sendo o uso de um valor padrão mais comum. Com base nessa contextualização, os objetivos desta tese são: (i) avaliação da correlação entre propriedades hidráulicas do solo, medidas em laboratório e parâmetros que quantificam o espaço de poros do solo a partir de imagens 3D obtidas por microtomografia de raios X; (ii) a análise funcional da parametrização das propriedades hidráulicas do solo na predição dos componentes do balanço hídrico do solo por um modelo agro-hidrológico. Para a verificação da relação entre as propriedades hidráulicas do solo e os parâmetros da imagem do solo, foi realizada uma análise de regressão múltipla entre os parâmetros do espaço poroso por imagens e parâmetros empíricos do modelo semi-determinística, obtidos com experimentos de evaporação juntamente com método de solução inversa. A avaliação funcional das parametrizações hidráulicas do solo foi feita pela análise de a sensibilidade das saídas de um modelo agro-hidrológico a várias maneiras de obter o parâmetro de tortuosidade/conectividade: aplicando um valor fixo comumente utilizado ou determinando seu valor em experimentos de evaporação no laboratório com tensiômetros na faixa úmida, tensiômetros na faixa seca, ou com tensiômetros nas faixas seca e

úmida. As simulações com o modelo agro-hidrológico foram realizadas por vários anos com disponibilidade de água distinta. A curva de retenção de solo obtida através de imagens do solo está em concordância com a curva de retenção obtida pelo experimento de evaporação, embora a limitação da resolução espacial da microtomografia, permitiu apenas quantificar macroporos, conseqüentemente, a determinação das propriedades hidráulicas em uma pequena faixa próxima à saturação. A parametrização hidráulica do solo usando uma faixa mais ampla de tensões é recomendada para melhor representar os processos na zona não-saturada e das relações solo-água-planta.

**Palavras-chave:** Propriedades hidráulicas do solo. Experimento de evaporação. Microtomografia. Imagens do solo 3D.

## LIST OF FIGURES

Figure 2.1 – Volumetric water content as a function of matric potential (I – data acquired from image analysis, EE – data acquired with water-based method (Hyprop tensiometers).....	35
Figure 2.2 – Hydraulic conductivity functions for the four evaluated soils. Different symbols indicate the three samples per soil. Lines are fits of equation 2.6 to the data points .....	36
Figure 2.3 – Observed versus predicted hydraulic parameters using a multiple regression analysis of image data.....	41
Figure 3.1 – Rainfall, maximum temperature ( $T_{max}$ ) and minimum temperature ( $T_{min}$ ) observed at the Piracicaba weather station during the wet (1995), average (2011) and dry (2014) cropping seasons used in simulations .....	53
Figure 3.2 – Volumetric water content as function of soil matric potential for each soil; dots represent measured values and lines are fits.....	58
Figure 3.3 – Unsaturated hydraulic conductivity as function of soil matric potential; dots represent measured values and lines are fits.....	59
Figure 3.4 – Pressure head simulated at 10 cm depth for the Rhodic Nitossol during the wet, average and dry year. Horizontal lines represent the Feddes threshold pressure heads $h_2$ , $h_3$ and $h_4$ .....	62
Figure 3.5 – Simulated pressure head at 10 cm depth for the Rhodic Ferralsol, Rhodic Lixisol, Xanthic Ferrasol and Rhodic Nitossol during the average year .....	64
Figure 3.6 – Predicted relative maize yield for the Rhodic Nitossol for the wet, average and dry year using the five different parameterizations .....	66
Figure 3.7 – Predicted relative maize yield for the Rhodic Ferralsol, Rhodic Lixisol, Xanthic Ferrasol and Rhodic Nitossol for the average year using the five different parameterizations...	66



## LIST OF TABLES

Table 2.1 – Soil physical characteristics (average values $\pm$ standard deviation from X samples) .....	26
Table 2.2 – 3D X-ray image parameters at low and high spatial resolution in the four analyzed soils Rhodic Ferralsol, Rhodic Lixisol, Xanthic Ferralsol and Rhodic Nitosol (three samples per soil) .....	32
Table 2.3 – Fitting parameters for Van Genuchten equations .....	38
Table 2.4 – Spearman correlation matrix .....	39
Table 2.6 – p-values (5%) matrix of Spearman correlation .....	40
Table 3.1 – Bulk density ( $D_b$ ), particle density ( $D_p$ ), particle size distribution and geographical location of the four sampled soils .....	50
Table 3.2 – Threshold pressure head values of the Feddes, Kowalik and Zaradny (1978) reduction function for maize according to Taylor and Ashcroft (1972).....	54
Table 3.3 – Optimized van Genuchten-Mualem parameters (Eqs. 3.1 and 3.2) for the sampled soils, and RMSE values .....	55



## CONTENTS

1 INTRODUCTION .....	19
2 SOIL HYDRAULIC PARAMETERS AND 3D IMAGES ANALYSIS OF TROPICAL SOILS .....	23
2.1 Introduction.....	23
2.2 Material and methods.....	25
2.2.1 Soil material.....	25
2.2.2 X-ray CT scanning.....	26
2.2.3 Image Processing.....	27
2.2.4 Image Analysis.....	27
2.2.5 Retention curve from soil images.....	29
2.2.6 Evaporation method.....	30
2.2.7 Correlation of parameters and multiple regression .....	31
2.3 Results and Discussion.....	31
2.3.1 Image parameters.....	31
2.3.2 Soil hydraulic properties.....	33
2.3.3 Correlation between image parameters and hydraulic parameters.....	39
2.4 Conclusions.....	42
References.....	42
3 FUNCTIONAL EVALUATION OF SOIL HYDRAULIC PARAMETERIZATION IN SOME TROPICAL SOILS .....	47
3.1 Introduction.....	47
3.2 Material and Methods.....	49
3.2.1 Soil sampling.....	49
3.2.2 Experiments.....	50
3.2.3 Soil hydraulic parameterization (SHP) .....	51
3.2.4 Agro-hydrological simulations.....	52
3.3 Results and Discussion.....	54
3.3.1 Soil hydraulic parameterization.....	54
3.3.2 Agro-hydrological simulations.....	60
3.4 Conclusions.....	67
References.....	68



## 1 INTRODUCTION

Prediction of soil water state and movement of water in the soil is one of the most subjects studied in soil physics. The importance of this theme is attached to processes related to availability of water to plants, transport of solutes in the soil, irrigation and drainage management, soil and water conservation, among others. Besides these, there is the direct influence of the state and soil water balance on its thermal and gaseous regime. Knowledge of soil water properties (retention and water conductivity) is essential for any modeling in hydrology, meteorology and plant production, since these properties are key elements in the fundamental equations involved and, therefore, in the quantification of forecasts soil water flow.

Soil water retention and soil hydraulic conductivity express, respectively, the relationship between storage and energetic state of water, and the easiness with which water is conducted through the soil. Several factors interfere in soil retention capacity, one of those factor is the grain size distribution, since it defines the area of contact between solid particles and water and determines the pore size distribution. Another important factor in water retention is the soil structure, as it characterizes the arrangement of the particles and, consequently, the pore space geometry.

In order to characterize the soil water retention, the water content and its specific or potential energy are correlated; this functional relationship is usually called retention curve and can be correlated with the soil pore diameter distribution. The relationship between the soil hydraulic conductivity and its water content or potential, in turn, is determined by the geometry and continuity of its pores filled with water, thus becoming dependent on its shape, quantity, distribution and continuity. Indirect methods to obtain saturated hydraulic conductivity may presume mathematical relationships and correlations between the saturated hydraulic conductivity,  $K_s$ , and other non-hydraulic soil variables, such as soil density, total porosity, macro and microporosity, which influence the distribution of the pores and, consequently, the permeability of soils.

Among the methods to determine the soil hydraulic conductivity in function of water content or matric potential, there are field methods (instant profile, impermeable layers), laboratory (internal drainage, hot air, evaporation) and empirical methods, based on pores diameters distribution.

Evaporation method, also called Wind method in homage to its proposer (WIND, 1968), is a laboratory method that is based on the water evaporation of a sample, allowing to simultaneously determine the retention curve,  $h(\theta)$ , and hydraulic conductivity as a function of water content or matric potential,  $K(\theta, h)$ . The determination is carried out under controlled measurement conditions and presents good performance, even in soils with low hydraulic conductivity. It consists of subjecting an initially saturated soil cylinder to a progressive drying during which it is analyzed: (i) the temporal variation of soil mass  $m(t)$  in the cylinder to determine the rate of water loss by evaporation and (ii) The evolution of the matrix potential values  $h(z, t)$  of the water in the soil, in some vertical positions in the sample as a function of time. For mass determination, the experimental set is placed on a self-registering scale. The potential of water is usually monitored with microtensiometers.

Wind methods advantages are: (i) in any measurement time, only mean water content of the sample needs to be determinate; (ii) the curves  $h(\theta)$  and  $K(\theta, h)$  can be estimated simultaneously; and (iii) as discrete values of water content and hydraulic conductivity are calculated, it is not necessary to infer about an adjustment mathematical model of water relations

In addition to experimental techniques involving water movement itself, unsaturated soil hydraulic conductivity can also be predicted from the geometry of the porous system (CHILDS; COLLIS-GEORGE, 1950; BURDINE, 1953; MUALEM, 1976) with the use of water retention curve (BROOKS; COREY, 1964; MUALEM, 1976; van GENUCHTEN, 1980).

Alternatively, to the direct conductivity determination methods described above, the pore space may also be characterized by tomography. This characterization may allow an estimation of the hydraulic conductivity. The microtomography (X-ray) or  $\gamma$ -ray microtomography is a non-destructive technique that can be efficiently used in studies related to soil structure. It allows cross sections visualization of samples interior without having to cut them or make any other type of invasion. The  $\mu$ TC technique uses the principle of radiation attenuation in media material, being the basic idea the image reconstruction of a section of the sample, through its projections in several directions. These projections are obtained by sweeping the sample with a radiation beam and measuring its attenuation. A matrix of data is thus formed which is processed in a personal computer, obtaining the image in the beam plane section.

X-ray tomography has been used in the field of soil science since the early 1980s, and presents several advantages for pore space characterization: it allows a relatively quick measurement acquisition; it is non-destructive; and the resolution can reach micron scale or less. An increasing number of publications refers to this technique, along with new algorithms to enhance analyses and perform original measurements, such as pore size distribution, shape, connectivity or orientation. Soil processes can be simulated in a 3D porous space using dynamic models and X-ray computed tomography images; examples include water flow, predict soil hydraulic conductivity, fungal colonization in the pore space or organic matter decomposition.

The objectives of work were (i) evaluation of the correlation between soil hydraulic properties, measured in the laboratory, and images parameters that quantifies soil pore space through 3D images obtained by X-ray microtomography; and (ii) adequacy analysis of soil hydraulic properties parameterization in the prediction of soil hydraulic processes and identify the effect on agrohydrological simulations.

## References

BROOKS, R.H.; COREY, A.T. **Hydraulic properties of porous media**. Fort Collins, CO: Colorado State University, 1964. (Hydrology Paper, 3).

BURDINE, N.T. Relative permeability calculations from pore size distribution data. **Transactions of Society for Mining, Metallurgy, and Exploration**, Littleton, CO, v. 198, p. 71–77, 1953.

CHILDS, E.C.; COLLIS-GEORGE, N. The permeability of porous materials. **Proceedings of the Royal Society of London. Series A: Mathematical and Physical Sciences**, London, v. 201, p. 392–405, 1950.

MUALEM, Y. A new model for predicting the hydraulic conductivity of unsaturated porous media. **Water Resources Research**, Hoboken, v. 12, p. 513-522, 1976.

VAN GENUCHTEN, M.T. A closed-form equation for predicting the hydraulic conductivity of unsaturated soils. **Soil Science Society of America Journal**, Madison, v. 44, p. 892-898, 1980.

WIND, G.P. Capillary conductivity data estimated by a simple method. In: RIJTEMA, P.E.; WASSINK, H. (Ed.). **Water in the unsaturated zone**. Louvain, Belgium: UNESCO; International Association of Scientific Hydrology, 1968. v. 1.



## 2 SOIL HYDRAULIC PARAMETERS AND 3D IMAGES ANALYSIS OF TROPICAL SOILS

### Abstract

Transport processes of compounds in the soil are related and strongly dependent on pore space structure and geometry. A better description and comprehension of transport processes in soils requires a better characterization at the pore scale. It is common practice to determine hydraulic properties (conductivity and retentivity) in lab experiments that are labor intensive and time consuming. X-ray computerized microtomography is a fast and non-destructive technique that allows visualization of soil structures, offering a potential tool for understanding soil structure and its relation to transport properties. Coupling soil hydraulic property measurements and X-ray CT, we evaluated the correlation between soil hydraulic properties measured in undisturbed samples using evaporation experiments and 3D X-ray microtomography image properties; a stepwise multiple regression analysis was performed that allows to predict hydraulic parameters from image parameters.

**Keywords:** connectivity, pores, ImageJ

### 2.1 Introduction

Soil structure is considered a main attribute determining soil quality and its qualitative role in soil hydrology is well documented on the pedologic scale. Soil macro- and micromorphology is intrinsically related to soil structure given by pore space and spatial distribution, being considered as the basis for explaining the influence of soil structure on hydraulic functions (KUTÍLEK, 2004) as well as on mechanical characteristics (VOGEL; WELLER; SCHLÜTER, 2010).

Natural soils are porous media containing complex structures at several length scales. The micro-scale, also referred to as the pore-scale, is the scale at which individual grains and fluid interfaces can be resolved and identified and at which many physical and chemical phenomena are rooted. Larger-scale processes are often governed by these small-scale phenomena (WILDENSCHILD; SHEPPARD, 2013). The flow of water through soil is controlled by the size, shape and connection of pores, which is in turn controlled by the size and packing of soil particles.

For soil water dynamic properties, pore system continuity is often more important than pore diameters (BERALDO; SCANNAVINO JUNIOR; CRUVINEL, 2014). Bouma (1982) highlighted the importance of pore continuity for the flow of water and solutes in the soil, emphasizing that small pores often enhance soil hydraulic conductivity since they form a continuous network, while large pores cannot contribute to flow in the case of discontinuity.

Traditionally, porosity is characterized using soil bulk density and water retention data (EVERTS; KANWAR, 1992). Whereas these measurements are an indirect measure of pore size distributions or porosity, they do not include any information on the spatial distribution of the pores, on the nature of the pore space or on pore connectivity and continuity (GANTZER; ANDERSON, 2002). More insight in soil pore space can be obtained by measuring hydraulic conductivity, both saturated and unsaturated. The relation between hydraulic conductivity and water content or pressure head allows to infer about pore connectivity and continuity, by the introduction of an empirical parameter to account for eccentricity of the flow path (CHILDS; COLLIS-GEORGE, 1950; BURDINE, 1953; MUALEM, 1976).

Among the water-based methods for determination of soil hydraulic properties, the Wind (1968) evaporation method is a frequently employed one (ŠIMŮNEK; WENDROTH; VAN GENUCHTEN, 1998; SCHINDLER; MÜLLER, 2006; PETERS; DURNER, 2008; PINHEIRO; VAN LIER; METSELAAR, 2017). It is a laboratory method based on the evaporation of water from a soil sample, allowing the simultaneous determination of the retention curve  $h(\theta)$  and the hydraulic conductivity property  $K(\theta, h)$  during the natural desiccation of the soil. The calculation procedure evolved from a manually assisted iterative routine (WIND, 1968) to modern inverse modeling techniques (ŠIMŮNEK; WENDROTH; VAN GENUCHTEN, 1998; SCHNEIDER et al., 2006).

Besides the indirect water-based measurement of pore geometry characteristics, the characterization of soil pore space can also be achieved by the direct observation of pores and features using microscopic thin-section 1D techniques or by X-ray or gamma ray microtomography yielding 2D or 3D images. These techniques allow to visualize the pores within the technically possible resolution of each method and equipment used. Through 3D images, it is possible to observe the geometry and spatial arrangement, enabling to visualize and quantify pore connectivity and continuity.

The computer-assisted quantification of pore size distribution from soil images may be useful to improve understanding of macroporosity and how it relates to tension and hydraulic conductivity. The pore size distribution derived from microtomography may allow to better describe near-saturated hydraulic properties (BECKERS et al., 2014), as an accurate description

of the retention curve in the wet range is a challenge due to difficulties in determining precisely soil water content at lower pressure heads near saturation (VERECKEN et al., 2010). These authors also pointed out the drawbacks of exact measurements in the change of water content at low pressure heads.

Traditional methods for the determination of hydraulic properties are often limited to relatively narrow ranges of water content. On the other hand, microtomography technique allows a relatively quick measurement acquisition; it is a non-destructive technique, providing a detailed view into the physical structure of undisturbed soil at a spatial resolution of a few microns. It is very promising due to its versatility, being applied in several areas, specifically in soil science for the representation and morphological quantification of porous space. The joint use of hydraulic properties and visual quantification of pore space may be helpful for a better parameterization and understanding of soil properties and behavior. Therefore, in order to verify the relation between soil hydraulic properties and soil image parameters that describe the pore space, we analyzed soil images using microtomography as well as traditional water-based determination techniques.

## **2.2 Material and methods**

### **2.2.1 Soil material**

Undisturbed and disturbed samples were collected from the subsurface layer (0.10 – 0.30 m depth) of four soils from São Paulo State, Brazil: a Rhodic Ferralsol (coordinates 23° 06' 17" S; 46° 56' 01" W), a Rhodic Lixisol (23° 06' 32" S; 46° 55' 54" W), a Xanthic Ferrasol (22° 42' 51" S; 47° 37' 02" W), and a Rhodic Nitossol (22° 42' 02" S; 47° 37' 22" W). Undisturbed samples were collected in PVC cylinders (12 samples, 7.5 cm diameter, 7.5 cm high) for CT analysis as well as in metal rings (64 samples, 5 cm diameter, 3 cm high) for water-based analyses. The samples were stored under refrigeration at field-moist condition (i.e. not air dry to avoid structural changes due to shrinkage) and without mechanical disturbance. Soil-particle density was determined by pycnometry using disturbed samples. Results are summarized in Table 2.1.

Table 2.1 – Soil physical characteristics (average values  $\pm$  standard deviation from 8 samples)

	Soil			
	Rhodic Ferralsol	Rhodic Lixisol	Xanthic Ferralsol	Rhodic Nitosol
Bulk density $D_b$ (kg m <sup>-3</sup> )	1506 $\pm$ 85	1336 $\pm$ 88	1851 $\pm$ 54	1547 $\pm$ 60
Particle density $D_p$ , (kg m <sup>-3</sup> )	2577 $\pm$ 67	2548 $\pm$ 34	2590 $\pm$ 57	2822 $\pm$ 142
Total Porosity, (m <sup>3</sup> m <sup>-3</sup> )	0.416 $\pm$ 0.076	0.476 $\pm$ 0.061	0.286 $\pm$ 0.055	0.452 $\pm$ 0.101
Saturated hydraulic conductivity $K_s$ , (m d <sup>-1</sup> )	2.85 $\pm$ 1.74	3.15 $\pm$ 2.88	0.030 $\pm$ 0.049	0.624 $\pm$ 0.36
Grain size distribution				
Sand content (kg kg <sup>-1</sup> )	0.603	0.678	0.754	0.346
Silt content (kg kg <sup>-1</sup> )	0.071	0.076	0.024	0.253
Clay content (kg kg <sup>-1</sup> )	0.326	0.246	0.222	0.401
FAO texture class	Sandy clay loam	Sandy clay loam	Sandy clay loam	Clay

### 2.2.2 X-ray CT scanning

Samples taken in the PVC rings were submitted to image acquisition with a CT system Nikon XT H 225, with the following technical specifications: dual reflection-transmission target system including a 225 kV, 225 W high performance X-ray source, equipped with a reflection target with spot size of 3  $\mu$ m combined with a nano-focus transmission module, spot size of 1  $\mu$ m.

The images were acquired in two steps, using copper filters to minimize artifacts; filter thickness was dependent on the soil type. The first step comprised the imaging of the entire sample at low spatial resolution (pixel size 40  $\mu$ m, energy settings 150 kV and 280 – 419  $\mu$ A). The second step aimed to acquire the image of a region of interest inside the sample, scanning at high spatial resolution (pixel size of 12  $\mu$ m, energy settings 115 – 190 kV and 80 – 288  $\mu$ A), allowing an improved visualization of smaller pores.

After the image acquisition, median filters were applied before reconstruction in order to reduce random noise from the detector. Median filters consist of a nonlinear smoothing method used to reduce isolated noise without blurring sharp edges (LEE et al., 2013). Reconstruction was done with the software CT Pro 3D (Nikon) and saved in raw format (tiff) and 8-bit gray scale resolution.

### 2.2.3 Image Processing

Image processing was performed with the image analysis software FIJI/Image J (SCHINDELIN et al., 2012). Initially, the images were submitted to the preprocessing step in which covering denoising, edge enhancement, artifact removal and intensity bias correction were applied over the images. The adaptive filter (OLLION et al., 2013) available in ImageJ was used for noise removal.

The segmentation process provides a way to separate the object of interest from the background, in this case, the pore space from the soil matrix. This step was performed using the ImageJ thresholding tool (automated segmentation) which applies the local thresholding method combined with Histogram analysis. The local thresholding values are determined in a local environment (often defined by the radius of a circular neighborhood) and the local cut-off values are locally applied to the individual pixels of the image. Thus, darker areas in an image might be extractable comparably as well as very bright areas, but this would not be possible with a global threshold only, where specifically very dark areas shift into the background or might be under-extracted. More information about segmentation methods can be found in Iassonov, Gebrenegus and Tuller (2009).

After the segmentation process, morphological operations of erosion-dilation were applied into binary images. Erosion-dilation is a mathematical technique to find the skeleton of the pore space, the skeleton runs through the centers of the pores and throats and defines the topology (LINDQUIST; VENKATARANGAN, 1999; LINDQUIST et al., 2000).

### 2.2.4 Image Analysis

Image analysis consisted of calculating the  $\chi$  density, macroporosity ( $MP$ ), Gama ( $\Gamma_a$ ) and pore surface area density ( $SA$  density) as specified in the following, using results from the BoneJ algorithm implemented in ImageJ.

#### **$\chi$ density (connectivity density)**

$\chi$  density ( $\text{mm}^{-3}$ ) was calculated by the quotient of the Euler number ( $\chi$ ) and the volume of the image ( $\text{mm}^3$ ). As soil images with two spatial resolutions were available, the transformation of the Euler number into  $\chi$  density allows to compare the values without bias, since when doing this operation, the dependence of the spatial resolution is removed.

The Euler number ( $\chi$ ), also called the Euler-Poincaré characteristic, describes the shape or structure of a topological space regardless of the way it is bent. The Euler number is one of the Minkowski functionals and a topological measure used for describing the connectivity of spatial structures (ARNS; KNACKSTEDT; MECKE, 2002; VOGEL; ROTH, 2001; VOGEL; WELLER; SCHLÜTER, 2010). In 3D, the Euler number is calculated as:  $\chi = N - C + H$ , where  $N$  is the number of isolated pores,  $C$  is the number of redundant connections or loops within the pore space often referred as connectivity or genus and  $H$  is the number of completely enclosed cavities in the considered soil volume (VOGEL, 1997, VOGEL; ROTH, 2001). Increasing positive values of the Euler number indicate decreasing connectivity of the structure, and decreasing negative values indicate increasing connectivity (VOGEL, 1997).

The algorithm uses voxel neighborhoods to calculate the Euler number of the volume and adjusts this to give the contribution of the volume to the connectivity of the structure it was obtained from. Toriwaki and Yonekura (2002) present fundamental properties of topological structure of a 3D digitized picture and provide a method to treat topology of digitized 3D figure.

### **Macroporosity ( $MP$ )**

Macroporosity was obtained by the determination of the volume occupied by pores relative to the total image volume. For the images with low spatial resolution, only pores larger than 40  $\mu\text{m}$  can be visualized; and for the images with high spatial resolution, pores larger than 12  $\mu\text{m}$  can be visualized and quantified.

### ***SA density***

Pore surface area density (*SA density*,  $\text{mm}^{-1}$ ) was calculated by the sum of the pore surface area ( $\text{mm}^2$ ) of each individual pore and divided by the image volume ( $\text{mm}^3$ ). The algorithm measures the pore surface area from a surface mesh.

### **Gama ( $\Gamma_a$ )**

Gama ( $\Gamma_a$ ) is a dimensionless connectivity indicator for a specific phase (RENARD; ALLARD, 2013) indicating individual pore clusters calculated by:

$$\Gamma_a = \frac{1}{N_a^2} \sum_{i=1}^{N_i} n_i^2 \quad 2.1$$

where each cluster of phase  $a$  has a label  $i$  and a size  $n_i$ ,  $N_i$  is the number of clusters and  $N_n$  is the number of all phase  $a$  voxels.

$\Gamma_a$  has a lower value when the porous system presents several isolated and non-connected clusters of macropores; however, if the porous system is dominated by at least one large interconnected macropore,  $\Gamma_a$  has large value. Cluster labeling is typically achieved with a fast method by Hoshen and Kopelman (1976).  $\Gamma_a$  has the advantage over the popular Euler number that it is bounded by [0, 1] and less sensitive to noise (SCHLÜTER et al., 2014; SCHLÜTER; VOGEL, 2016).

### 2.2.5 Retention curve from soil images

The pores-size distribution was computed with the maximum inscribed sphere method as implemented in BoneJ from ImageJ (HILDEBRAND; RÜEGSEGGER, 1997; DOUGHERTY; KUNZELMANN, 2007; DOUBE et al., 2010), where the pore radii were determined by the volume of the inscribed sphere.

In order to obtain the  $\theta$ - $h$  relation, pore diameters were transformed into pressure head  $h$  according to the Young-Laplace equation:

$$h = \frac{2\sigma \cos\alpha}{\rho g r} \quad 2.2$$

where,  $\sigma$  is the water surface tension ( $\sigma = 0.073 \text{ N m}^{-1}$  at  $20 \text{ }^\circ\text{C}$ ),  $\alpha$  is contact angle (normally considered to be  $0^\circ$  for pure water and clean mineral surfaces),  $\rho$  is the water specific gravity ( $\rho = 1000 \text{ kg m}^{-3}$ ),  $g$  is gravity ( $g = 9.81 \text{ m s}^{-2}$  at the Earth surface), and  $r$  is the pore radius [m]. The volumetric water content,  $\theta$ , was assumed to be equal to the volume occupied by the correspondent pore relative to the total volume.

Hydraulic properties were expressed according to the Van Genuchten – Mualem equations (VAN GENUCHTEN, 1980):

$$S_e = \frac{\theta - \theta_r}{\theta_s - \theta_r} = \left[ 1 + (\alpha|h|)^n \right]^{\frac{1}{n}-1} \quad 2.3$$

where  $S_e$  is the effective saturation,  $\theta$  is the water content,  $\theta_s$  is the saturated water content;  $\theta_r$ , residual water content;  $\alpha$  and  $n$  are empirical constants affecting the shape of the retention curve;  $l$  is a pore-connectivity parameter. The parameters for Equation 2.3 were obtained with the nonlinear least-squares optimization program RETC (VAN GENUCHTEN; LEIJ; YATES, 1991; YATES et al., 1992).

### 2.2.6 Evaporation method

For water-based determinations, a simultaneous measurement of  $\theta(h)$  and  $K(h)$  was conducted using the evaporation method of Schindler (1980), a simplification of the Wind (1968) approach. The simplified method of Schindler uses pressure head measurements,  $h_1$  and  $h_2$ , at only two different depths,  $z_1$  and  $z_2$ . The same undisturbed soil samples used for image acquisition, taken in the PVC rings, was employed for the evaporation experiment. Samples were slowly saturated by capillarity, after which two Hyprop tensiometers (HYdraulic PROPerTy analyzer, UMS, Munich) (SCHINDLER et al., 2010) were vertically inserted in the sample through drilled holes with centers at 50 ( $z_1$ ) and 25 mm ( $z_2$ ) vertical distance from the sample bottom. The sample was sealed at the bottom and placed on a balance, leaving the surface free to evaporate. Tensions ( $h$ ) at two heights and sample masses ( $M$ ) were measured at pre-determinate time intervals. The hydraulic gradient ( $i_m$ ) was calculated from the tension values and the tensiometer distance. The flux density ( $q$ ) was derived from the soil water-mass difference  $\Delta M$  per surface area ( $A$ ) and time unit ( $\Delta t$ ). Single points of the water-retention curve were calculated based on water loss per volume of the core sample at time  $t$  and the mean tension in the sample at that time. The hydraulic conductivity ( $K$ ) was calculated by

$$K(\bar{h}) = \frac{\Delta V}{2A \Delta t i_m} \quad 2.4$$

where  $\bar{h}$  is the mean tension, averaged over the upper and the lower tensiometer and the time interval,  $A$  is the cross-sectional area of the sample,  $\Delta V$  is the mass of evaporated water in time interval  $\Delta t = t_2 - t_1$ ,  $\rho$  is the density of water, and  $i_m$  is the mean hydraulic gradient in the interval, given by

$$i_m = \left( \frac{ht_{1,z_1} - ht_{1,z_2}}{2\Delta z} + \frac{ht_{2,z_1} - ht_{2,z_2}}{2\Delta z} \right) - 1 \quad 2.5$$

where  $ht_{t,z_1,z_2}$  indicates the tension at 50 mm and at 25 mm values at times  $t_1$  and  $t_2$ , respectively, and  $\Delta z$  is the vertical distance between the tensiometer positions.

Hydraulic properties were expressed according to the Van Genuchten – Mualem equations (VAN GENUCHTEN, 1980), equation 2.3 for retention and for hydraulic conductivity  $K$ :

$$K = K_s S_e^l \left\{ 1 - \left[ 1 - (S_e)^{\frac{n}{n-1}} \right]^{1-\frac{1}{n}} \right\}^2 \quad 2.6$$

where  $K_s$  is the hydraulic conductivity at saturation and  $l$  is a pore-connectivity parameter. To obtain the fitting parameters, Equations 2.3 and 2.6 were simultaneously fitted to the data from the evaporation experiments.

The hydraulic conductivity is affected by both by pore size distribution and by the continuity and tortuosity of flow path. The effects of these two factors is represented by the exponent  $l$  in Equation 2.6. In most studies,  $l$  is considered constant and equal to 0.5, as determined by Mualem (1976) on a dataset with 45 soils.

### 2.2.7 Correlation of parameters and multiple regression analysis

Spearman correlations were used to investigate the correlation between parameters from water-based hydraulic parameters and pore-space image parameters. The Spearman correlation matrix is used for non-parametric correlations, not requiring the assumption that the relationship between variables is linear, nor requiring quantitative variables (SIEGEL; CASTELLAN JÚNIOR, 2006).

For calibration of hydraulic parameters as a function of image parameters, eight samples were chosen randomly to perform a stepwise multiple regression analysis, thus obtaining the equation for each soil hydraulic parameter. The remaining four samples were used for validation, applying the calibrated equations to predict the soil hydraulic parameters and comparing those to the water-based hydraulic parameters.

## 2.3 Results and Discussion

### 2.3.1 Image parameters

Table 2.2 shows the pore space image parameters at low (40  $\mu\text{m}$ ) and high (12  $\mu\text{m}$ ) spatial resolution; as the images with high spatial resolution (12  $\mu\text{m}$ ) were obtained from preview images, only a portion of the sample volume was analyzed, resulting in different parameters values for both spatial resolutions.

Table 2.2 – 3D X-ray image parameters at low and high spatial resolution in the four analysed soils  
Rhodic Ferralsol, Rhodic Lixisol, Xanthic Ferralsol and Rhodic Nitosol (three samples per soil)

Lower spatial resolution (40 $\mu\text{m}$ )				
Sample	$MP$ ( $\text{m}^3 \text{m}^{-3}$ )	$SA$ density ( $\text{mm}^{-1}$ )	$\Gamma_a$	$\chi$ density ( $\text{mm}^{-3}$ )
Rhodic Ferralsol - Sandy clay loam				
1	0.09	0.22	0.95	-0.14
2	0.04	0.08	0.77	-0.10
3	0.06	0.13	0.89	-0.07
Mean $\pm$ SD	$0.06 \pm 0.03$	$0.14 \pm 0.07$	$0.87 \pm 0.09$	$-0.10 \pm 0.04$
Rhodic Lixisol - Sandy clay loam				
1	0.20	0.57	0.99	-0.79
2	0.11	0.29	0.97	-0.78
3	0.18	0.53	0.99	-0.98
Mean $\pm$ SD	$0.16 \pm 0.05$	$0.46 \pm 0.15$	$0.98 \pm 0.01$	$-0.85 \pm 0.11$
Xanthic Ferralsol - Sandy clay loam				
1	0.02	0.05	0.79	-0.11
2	0.05	0.85	0.13	-0.36
3	0.05	0.70	0.12	-0.14
Mean $\pm$ SD	$0.04 \pm 0.02$	$0.53 \pm 0.43$	$0.35 \pm 0.38$	$-0.20 \pm 0.14$
Rhodic Nitosol - Clay				
1	0.14	0.40	0.99	-0.62
2	0.10	0.30	0.98	-0.52
3	0.11	0.34	0.99	-0.51
Mean $\pm$ SD	$0.12 \pm 0.02$	$0.35 \pm 0.05$	$0.99 \pm 0.01$	$-0.55 \pm 0.06$
Higher spatial resolution (12 $\mu\text{m}$ )				
Sample	$MP$ ( $\text{m}^3 \text{m}^{-3}$ )	$SA$ density ( $\text{mm}^{-1}$ )	$\Gamma_a$	$\chi$ density ( $\text{mm}^{-3}$ )
Rhodic Ferralsol - Sandy clay loam				
1	0.15	0.57	0.89	-0.45
2	0.03	0.24	0.67	-1.80
3	0.07	0.07	0.90	-1.81
Mean $\pm$ SD	$0.08 \pm 0.06$	$0.29 \pm 0.25$	$0.82 \pm 0.13$	$-1.35 \pm 0.78$
Rhodic Lixisol - Sandy clay loam				
1	0.25	1.29	0.99	-26.09
2	0.12	0.54	0.96	-5.90
3	0.18	1.52	0.98	-8.45
Mean $\pm$ SD	$0.18 \pm 0.07$	$1.12 \pm 0.51$	$0.98 \pm 0.02$	$-13.48 \pm 10.99$
Xanthic Ferralsol - Sandy clay loam				
1	0.04	0.73	0.37	-1.76
2	0.09	0.92	0.60	-13.08
3	0.18	1.43	0.96	-24.57
Mean $\pm$ SD	$0.10 \pm 0.07$	$1.03 \pm 0.36$	$0.64 \pm 0.30$	$-13.14 \pm 11.41$
Rhodic Nitosol - Clay				
1	0.18	1.08	0.98	-0.01
2	0.16	0.96	0.97	-5.31
3	0.17	1.24	0.97	-2.99
Mean $\pm$ SD	$0.17 \pm 0.01$	$1.09 \pm 0.14$	$0.97 \pm 0.01$	$-2.77 \pm 2.66$

Pore space heterogeneity affects results between samples at the two spatial resolutions, 40  $\mu\text{m}$  and 12  $\mu\text{m}$ , therefore, resulting in different values of pore space image parameters. Soil images obtained with spatial resolution of 12  $\mu\text{m}$  presented smaller values of the Euler number and, consequently, of  $\chi$  density, indicating a higher connectivity.

This result is expected, since a higher spatial resolution allows to visualize smaller pores, including packing pores and intra-aggregate pores; however, part of soil porosity is not quantified by the image analysis due to the spatial resolution restriction. Also, higher values of macroporosity were obtained on the images with the higher spatial resolution, since it is more likely for a macropore to occupy a larger fraction of the image volume.

Soil image parameters are also dependent of the threshold employed, therefore different threshold methods will result in different parameters values. Additionally, the method is somehow subjective and different results are expected to be obtained for different observers. Baveye et al. (2010) conducted an investigation to determine how much variation exists among the outcomes of various image thresholding strategies (including any image pre-treatment deemed appropriate), routinely adopted by soil scientists. The authors found out that experts rely on very different approaches to threshold images of soils and that there is observer bias associated with this thresholding; experts, relying on various combinations of subjective procedures (e.g., manual contrast adjustment, visual thresholding) and automated steps, produced thresholded images that in some cases vary significantly with respect to simple quantitative measures, like porosity.

### **2.3.2 Soil hydraulic properties**

Figure 2.1 shows the water retention data obtained from the microtomography images and from the evaporation experiments. Results are consistent with the results obtained with pore-size distribution from image analysis and measured retention data.

Due to image resolution, image analysis allows only the determination of the wet range of the curve. For images with 40  $\mu\text{m}$  spatial resolution, the lower pore radius is 49.4  $\mu\text{m}$ , corresponding to pressure heads of -0.30 m; and for images with 12  $\mu\text{m}$  spatial resolution, the lower pore radius is 24.3  $\mu\text{m}$ , corresponding to pressure heads of -0.61 m. Probably the non-identification/quantification of some smaller pores occurred due to the processes of segmentation and morphological operations, in which small individual pores are identify as solids or incorporated in a neighboring larger pore. In the binary image it is very difficult to obtain pores with spatial resolution size, because very small pores (with sizes close to the spatial resolution) join to other pores or are hidden in the process of both segmentation and morphological operation.

The part of the retention curve that can be measured using the water-based method with Hyprop tensiometers (*EE*) is limited by tensiometer specifications. In our experiments we were able to measure down to -10 m, so the drier range could not be quantified.

Hydraulic conductivity functions for soils Rhodic Ferralsol, Rhodic Lixisol, Xanthic Ferralsol and Rhodic Nitosol obtained from the evaporation experiments model fits are represented in Figure 2.2. In general, the Xanthic Ferralsol presents a lower hydraulic conductivity, corroborating with its high bulk density and sandy clay loam texture (Table 2.1); this soil also presents a higher dispersion for parameters  $n$  and  $\alpha$  (Table 2.3), which reflects in its retention (Figure 2.1) and hydraulic conductivity (Figure 2.2) curves. The variability may be due to natural soil spatial variability, indicating that the samples may have been smaller than the Representative Elementary Volume.

Parameter  $n$  ( $n > 1$ ) is related to the pore-size distribution, higher values being associated with a homogeneous pore size distribution;  $n$  influences the slope of the retention curve at its inflection, as seen for e.g. the Xanthic Ferralsol (Figure 2.1) with a high  $n$  (Table 2.3). Parameter  $\alpha$  is related to the inverse of the air-entry pressure and scales the retention curve along the x-axis. Higher values of  $\alpha$  scale the curve closer to the y-axis making the matric potential at inflection to increase and to correspond to larger pores. With respect to the hydraulic conductivity (Figure 2.2), for the Rhodic Lixisol, the high value of  $n$  for sample 3 (Table 2.3) made its values for  $K$  to be higher than for the other two samples; being also observed for sample 1 of the Rhodic Nitosol.

Figure 2.1 – Volumetric water content as a function of matric potential (I – data acquired from image analysis, EE – data acquired with water-based method (Hyprop tensiometers))

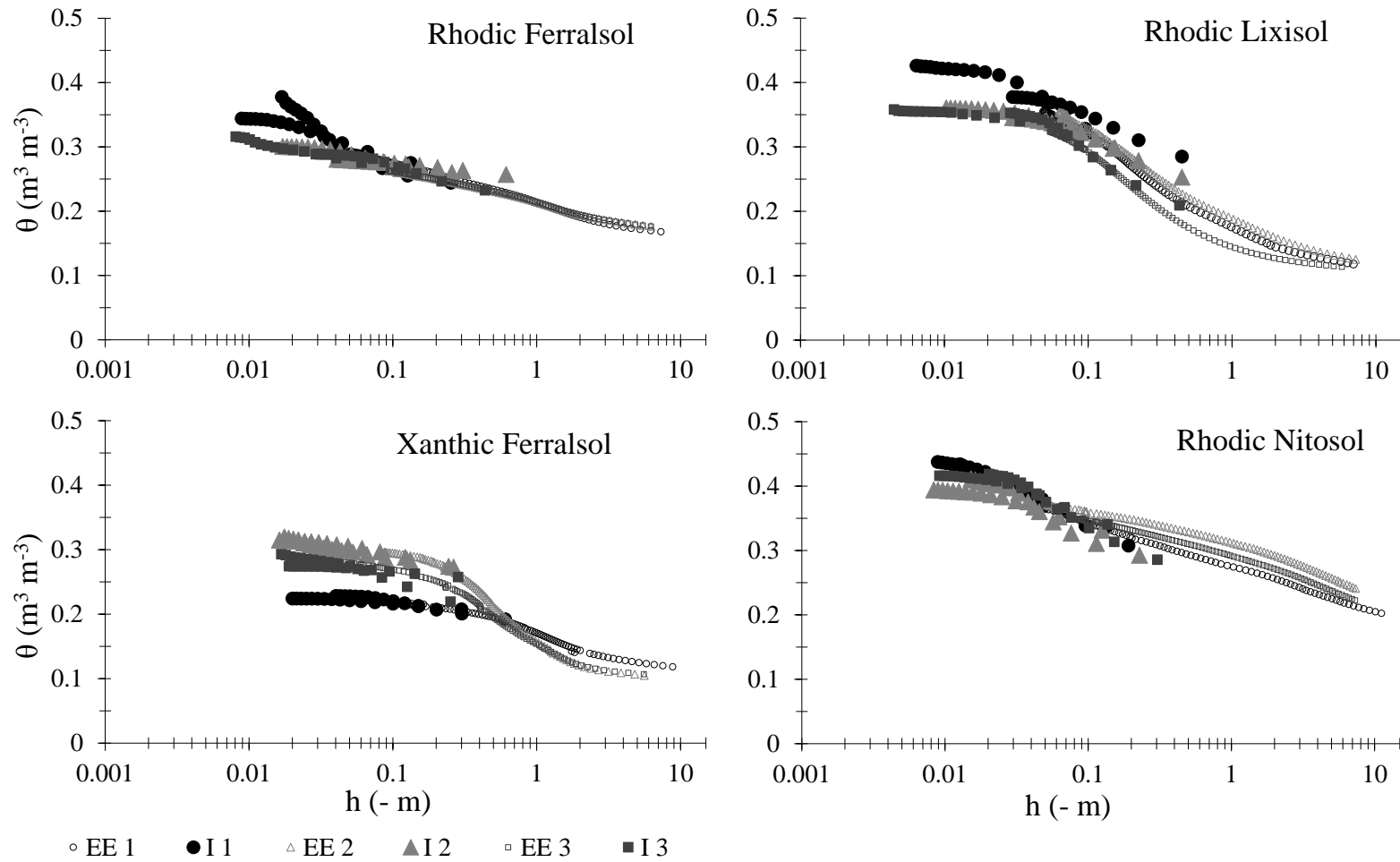
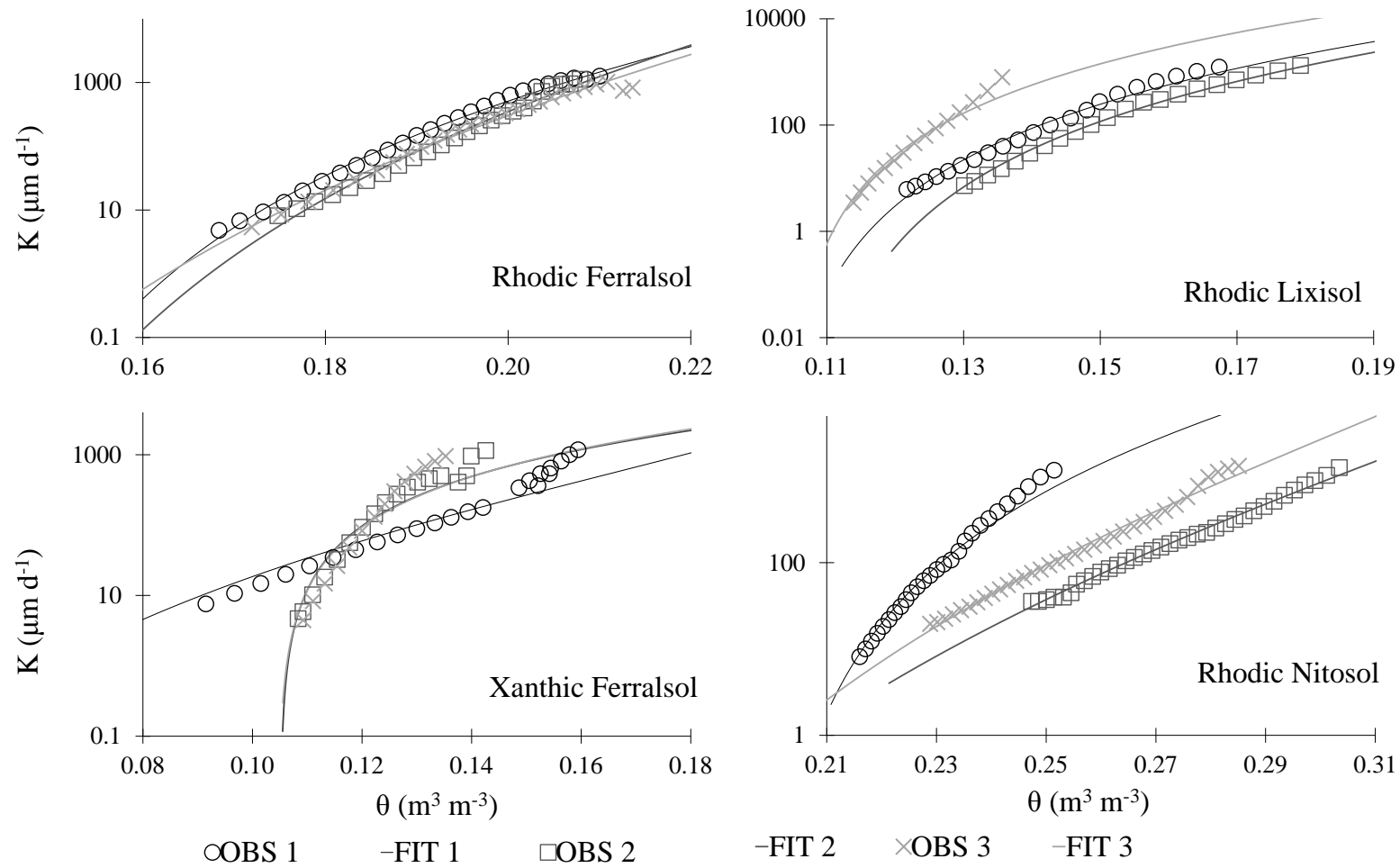


Figure 2.2 – Hydraulic conductivity functions for the four evaluated soils. Different symbols indicate the three samples per soil. Lines are fits of equation 2.6 to the data points



Fitting parameters for Equations 2.3 and 2.6 are shown in Table 2.3 (for the image analysis, hydraulic conductivity parameter  $l$  was not determined). It should be observed that parameters  $\theta_s$  and  $\theta_r$  are mere fitting parameters without clear physical meaning. The water content obtained by oven drying is defined as zero, and is normally less than  $\theta_r$ . Water contents below the residual water content  $\theta_r$  are physically possible but cannot be investigated with the empirical model used here.

Regarding the  $l$  parameter, observed values ranged from -1.68 to 1.49. Negative values for  $l$  are often reported (SCHUH; CLINE, 1990; KAVEH; VAN GENUCHTEN, 1992; YATES et al., 1992; KOSUGI, 1999; SCHAAP; LEIJ, 2000; OH; KIM; KIM, 2015; PINHEIRO; VAN LIER; METSELAAR, 2017). Schuh and Cline (1990) reported  $l$  varying between -8.73 and 14.80, for a data set of 75 soil samples. Schaap and Leij (2000) found  $l = -1$ , as optimal value that minimized the root mean square error for 235 soil samples from all texture range. A negative value of  $l$  implies in an increasing connectivity of water-filled pores with decreasing soil moisture content, which intuitively does not seem realistic (VERECKEN et al., 2010).

Although parameter  $l$  has been labeled an indicator of tortuosity and connectivity, its exact physical meaning is unclear (VOGEL, 2000; GHANBARIAN et al., 2013). Ghanbarian et al. (2013) discussed the concept of tortuosity, its varying definitions in the literature, and their significance. They also highlight the issue if tortuosity is an intrinsic property of the medium, of a process within the medium, or neither, being simply an adjustable parameter used to improve the agreement between theory and experiment. Because the tortuosity has a pronounced saturation dependence, tortuosity cannot simply be a property of the medium itself but must be derived from the actual paths of flow, conduction, or transport involved. Hoffmann-Riem, Van Genuchten and Flühler (1999) concluded that models based on Eq. (2.6) should not be interpreted as being physically based. Schaap and Leij (2000) also treat  $l$  as an empirical parameter.

Table 2.3 – Fitting parameters for Van Genuchten equations

Parameters						
Sample	$\theta_s$ (m <sup>3</sup> m <sup>-3</sup> )	$\theta_r$ (m <sup>3</sup> m <sup>-3</sup> )	$\alpha$ (m <sup>-1</sup> )	$n$	$l$	R <sup>2</sup>
Evaporation Experiment (EE)						
Rhodic Ferralsol – Sandy clay loam						
1	0.29	0.14	5.34	1.45	0.36	0.99
2	0.27	0.13	4.06	1.36	1.49	0.99
3	0.27	0.11	4.50	1.28	1.40	0.99
Rhodic Lixisol – Sandy clay loam						
1	0.37	0.10	8.04	1.66	-0.66	0.99
2	0.38	0.11	7.60	1.61	-0.75	1.00
3	0.35	0.10	8.59	1.83	-0.73	0.99
Xanthic Ferralsol – Sandy clay loam						
1	0.22	0.00	1.15	1.37	-1.22	0.96
2	0.29	0.11	2.25	2.60	-1.37	0.97
3	0.27	0.10	2.60	2.36	-1.53	0.95
Rhodic Nitosol – clay						
1	0.37	0.20	4.45	1.56	-1.41	0.97
2	0.37	0.10	2.86	1.20	-1.68	0.97
3	0.35	0.12	2.91	1.25	-0.44	0.97
Image analysis (I)						
Rhodic Ferralsol – Sandy clay loam						
1	0.35	0.26	26.31	3.66	–	0.89
2	0.31	0.25	45.22	1.73	–	0.93
3	0.32	0.03	66.56	1.10	–	0.95
Rhodic Lixisol – Sandy clay loam						
1	0.44	0.18	43.76	1.29	–	0.97
2	0.36	0.15	12.58	1.42	–	0.99
3	0.35	0.20	11.01	2.6	–	0.99
Xanthic Ferralsol – Sandy clay loam						
1	0.23	0.00	4.23	1.15	–	0.89
2	0.34	0.14	98.09	1.12	–	0.94
3	0.39	0.00	10538.58	1.06	–	0.70
Rhodic Nitosol – clay						
1	0.46	0.00	62.18	1.16	–	0.98
2	0.40	0.30	20.68	3.34	–	0.92
3	0.42	0.27	16.82	2.05	–	0.97

### 2.3.3 Correlation between image parameters and hydraulic parameters

Spearman's correlation evaluates the monotonic relationship between two continuous or ordinal variables. In a monotonic relationship, the variables tend to change together but not necessarily at a constant rate. The Spearman correlation coefficient is based on the graded values of each variable, rather than the data. The negative sign of correlation means that the variables vary in the opposite direction, that is, the higher categories of one variable are associated with lower categories of the other variable.

The Spearman correlation matrix (Table 2.4) and p-values (Table 2.5), at 5% of significance, show  $\theta_s$ ,  $\alpha$  and  $n$  to have a monotonic association between the variables.  $\theta_s$  and  $\alpha$  show a strong positive association with  $MP$ , while  $n$  was strongly associated to  $SA$  density.  $\theta_s$  showed a strong negative association with  $\chi$  density; parameters  $l$  and  $\theta_r$  weak association with any image pore space parameter.

Table 2.4 – Spearman correlation matrix

Parameters	$\theta_s$ ( $\text{m}^3 \text{ m}^{-3}$ )	$\theta_r$ ( $\text{m}^3 \text{ m}^{-3}$ )	$\alpha$ ( $\text{m}^{-1}$ )	$n$	$l$	$MP$ (%)	$SA$ density ( $\text{mm}^{-1}$ )	$\Gamma_a$	$\chi$ density ( $\text{mm}^{-3}$ )
$\theta_s$ ( $\text{m}^3 \text{ m}^{-3}$ )	1.00	0.16	0.52	0.05	-0.27	0.82	0.36	0.72	-0.85
$\theta_r$ ( $\text{m}^3 \text{ m}^{-3}$ )	0.16	1.00	0.19	-0.18	0.39	0.11	-0.12	0.12	0.15
$\alpha$ ( $\text{m}^{-1}$ )	0.52	0.19	1.00	0.13	0.45	0.73	0.04	0.61	-0.54
$n$	0.05	-0.18	0.13	1.00	-0.29	0.10	0.70	-0.22	-0.36
$l$	-0.27	0.39	0.45	-0.29	1.00	-0.01	-0.48	0.05	0.34
$MP$ (%)	0.82	0.11	0.73	0.10	-0.01	1.00	0.43	0.91	-0.86
$SA$ density ( $\text{mm}^{-1}$ )	0.36	-0.12	0.04	0.70	-0.48	0.43	1.00	0.12	-0.56
$\Gamma_a$	0.72	0.12	0.61	-0.22	0.05	0.91	0.12	1.00	-0.73
$\chi$ density ( $\text{mm}^{-3}$ )	-0.85	0.15	-0.54	-0.36	0.34	-0.86	-0.56	-0.73	1.00

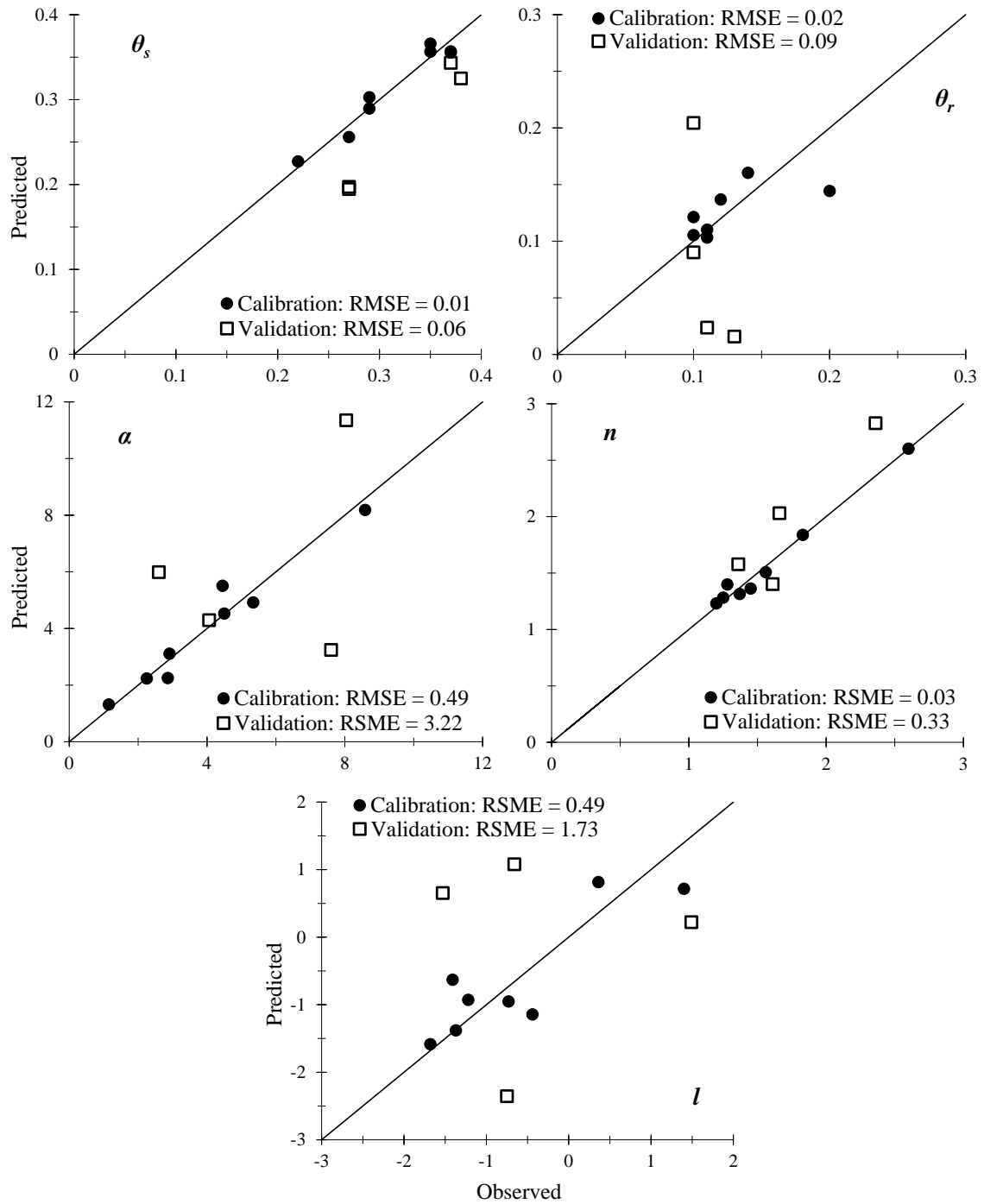
Table 2.5 – p-values (5%) matrix of Spearman correlation

Parameters	$\theta_s$ ( $\text{m}^3 \text{ m}^{-3}$ )	$\theta_r$ ( $\text{m}^3 \text{ m}^{-3}$ )	$\alpha$ ( $\text{m}^{-1}$ )	$n$	$l$	$MP$ (%)	$SA$ <i>density</i> ( $\text{mm}^{-1}$ )	$\Gamma_a$	$\chi$ <i>density</i> ( $\text{mm}^{-3}$ )
$\theta_s$ ( $\text{m}^3 \text{ m}^{-3}$ )	1.00	0.61	0.08	0.88	0.40	0.00	0.26	0.01	0.00
$\theta_r$ ( $\text{m}^3 \text{ m}^{-3}$ )	0.61	1.00	0.55	0.58	0.20	0.73	0.71	0.71	0.65
$\alpha$ ( $\text{m}^{-1}$ )	0.08	0.55	1.00	0.68	0.15	0.01	0.90	0.04	0.07
$n$	0.88	0.58	0.68	1.00	0.37	0.75	0.01	0.49	0.25
$l$	0.40	0.20	0.15	0.37	1.00	0.97	0.12	0.87	0.27
$MP$ (%)	0.00	0.73	0.01	0.75	0.97	1.00	0.16	0.00	0.00
$SA$ <i>density</i> ( $\text{mm}^{-1}$ )	0.26	0.71	0.90	0.01	0.12	0.16	1.00	0.71	0.06
$\Gamma_a$	0.01	0.71	0.04	0.49	0.87	0.00	0.71	1.00	0.01
$\chi$ <i>density</i> ( $\text{mm}^{-3}$ )	0.00	0.65	0.07	0.25	0.27	0.00	0.06	0.01	1.00

Observed hydraulic parameters obtained from the evaporation experiments and predicted parameters with stepwise multiple regression are plotted in Figure 2.3. Although  $l$  and  $\theta_r$  show weak correlations to image parameters of pore space, the prediction of those parameters using image data was performed and plotted, in order to show the accuracy and dispersion. Predicted values of  $\theta_s$  were underestimated, while the predicted values of  $n$  were overestimated. Results show that the employed statistical model (stepwise multiple regression) was not able to explain how pore space geometry relates to hydraulic property parameters, since for all hydraulic parameters the RMSE for validation was higher than the RMSE for validation.

The use of the Van Genuchten (1980) model assumes that the pore size distribution of the soil can be described by a single unimodal pore size distribution function, and that the pore system can be described as a bundle of capillaries with flow processes governed by the principles of capillary flow. Moreover, capillaries are filled either with water or with air, without accounting for film flow that may dominate in relatively dry soils (VERECKEN et al., 2010). These assumptions, allied to uncertainties concerning the physical meaning of  $l$  and limitations of the statistical model result in the low correlation between  $l$  and pore space image parameters.

Figure 2.3 – Observed versus predicted hydraulic parameters using a multiple regression analysis of image data



The prediction of soil hydraulic properties through CT image analysis is still a challenge, processes that occur in the soil depend on several factors that must be quantified and included with the characteristics of the pore space for an adequate prediction; along with the use of more complex hydraulic conductivity models that include information on the pore space shape and arrangement.

Quantification of soil characteristics through images is a powerful and promising technique, although there are still some limitations attached with the computer power, spatial resolution, lack of standard methodology to process and analyze soil images; this technique allows the quantification of several soil characteristics with only one image.

## 2.4 Conclusions

Determination of soil hydraulic parameters using image analysis may be performed in a small range close to saturation (-0.0045 to -0.61 m), due to the current limitation of the spatial resolution of the microtomograph.

Weak correlations were obtained between measured hydraulic parameters from the Van Genuchten model and pore space image parameters through stepwise multiple regression analysis, thus this statistical model was not able to explain how pore space geometry relates to hydraulic properties parameters from an empirical model.

## 2.5 References

ARNS, C.; KNACKSTEDT, M.; MECKE, K. Characterising the morphology of disordered materials. In: MECKE, K., STOYAN, D. (Ed.). **Morphology of Condensed Matter**. Berlin: Springer, 2002. p. 37–74. (Lecture Notes in Physics, 600).

BAVEYE, P.C.; LABA, M.; OTTEN, W.; BOUCKAERT, L.; STERPAIO, P.D.; GOSWAMI, R.R.; GRINEV, D.; HOUSTON, A.; HU, Y.; LIU, J.; MOONEY, S.; PAJOR, R.; SLEUTEL, S.; TARQUIS, A.; WANG, W.; WEI, Q.; SEZGIN, M. Observer-dependent variability of the thresholding step in the quantitative analysis of soil images and X-ray microtomography data. **Geoderma**, Amsterdam, v. 157, n. 1-2, p. 51-63, 2010.

BECKERS, E.; PLOUGONVEN, E.; GIGOT, N.; LÉONARD, A.; ROISIN, C.; BROSTAU, Y.; DEGRÉ, A. Coupling X-ray microtomography and macroscopic soil measurements: a method to enhance near-saturation functions? **Hydrology and Earth System Sciences Journal**, Munich, v. 18, p. 1805–1817, 2014.

BERALDO, J.M.G.; SCANNAVINO JUNIOR, F.A.; CRUVINEL, P.E. Application of x-ray computed tomography in the evaluation of soil porosity in soil management systems. **Engenharia Agrícola**, Botucatu, v. 34, n. 6, p. 1162-1174, 2014.

BOUMA, J. Measuring the conductivity of soil horizons with continuous macropores. **Soil Science Society of America Journal**, Madison, v. 46, p. 438-441, 1982.

DOUBE, M.; KŁOSOWSKI, M.M.; ARGANDA-CARRERAS, I.; CORDELIÈRES, F.P.; DOUGHERTY, R.P.; JACKSON, J.S.; SCHMID, B.; HUTCHINSON, J.R.; SHEFELBINE, S.J. BoneJ: Free and extensible bone image analysis in ImageJ. **Bone**, New York, v. 47, n. 6, p. 1076–1079, 2010.

DOUGHERTY, R.; KUNZELMANN, K.H. Computing Local Thickness of 3D Structures with ImageJ. **Microscopy and Microanalysis**, New York, v. 13(S02), p. 1678–1679, 2007.

EVERTS, C.J.; KANWAR, R.S. Interpreting tension-infiltration data for quantifying soil macropores: Some practical considerations. **Transactions of ASAE**, St. Joseph, v. 36, p. 423-428, 1992.

GANTZER, C.J.; ANDERSON, S.H. Computed tomographic measurement of macroporosity in chisel-disk and no-tillage seedbeds. **Soil and Tillage Research**, Amsterdam, v. 64, p. 101-111, 2002.

GHANBARIAN, B.; HUNT, A.G.; EWING, R.P.; SAHIMI, M. Tortuosity in Porous Media: A Critical Review. **Soil Science Society of America Journal**, Madison, v. 77, p. 1461–1477, 2013. doi:10.2136/sssaj2012.0435.

HILDEBRAND, T.; RÜEGSEGG, P. A new method for the model-independent assessment of thickness in three-dimensional images. **Journal of Microscopy**, Oxford, v. 185, p. 67–75, 1997.

HOFFMANN-RIEM, H.; VAN GENUCHTEN, M.T.H.; FLÜHLER, H. A general model of the hydraulic conductivity of unsaturated soils. In: INTERNATIONAL WORKSHOP ON CHARACTERIZATION AND MEASUREMENTS OF THE HYDRAULIC PROPERTIES OF UNSATURATED POROUS MEDIA, 1997, Riverside, CA. **Proceedings...** Riverside, CA: University of California, 1999. p. 31–42.

HOSHEN, J.; KOPELMAN, R. Percolation and cluster distribution. I. Cluster multiple labeling technique and critical concentration algorithm. **Physical Review. Part B**, College Park, v. 14, n. 8, p. 3438-3445, 1976.

IASSONOV, P.; GEBRENEGUS, T.; TULLER, M. Segmentation of X-ray computed tomography images of porous materials: A crucial step for characterization and quantitative analysis of pore structures. **Water Resources Research**, Hoboken, v. 45, n. 9, p. 1-12, 2009.

KAVEH, F.; VAN GENUCHTEN, M.T. A further look at a new unsaturated hydraulic conductivity equation. **Iranian Journal of Agricultural Science**, Tehran, v. 23, p. 24–32, 1992.

KOSUGI, K. General model for unsaturated hydraulic conductivity for soils with lognormal pore-size distribution. **Soil Science Society of America Journal**, Madison, v. 63, p. 270–277, 1999.

KUTÍLEK, M. Soil hydraulic properties as related to soil structure. **Soil & Tillage Research**, Amsterdam, v. 79, p. 175–184, 2004.

LEE, J.; LEE, U.; KIM, B.; YOON, J. A computational method for detecting copy number variations using scale-space filtering. **BMC Bioinformatics**, London, v. 14, n. 57, p. 1-16, 2013.

LINDQUIST, W.B.; VENKATARANGAN, A. Investigating 3D geometry of porous media from high resolution images. **Physics and Chemistry of the Earth, Part A: Solid Earth and Geodesy**, Oxford, v. 24, n. 7, p. 593–599, 1999.

LINDQUIST, W.B.; VENKATARANGAN A.; DUNSMUIR J.; WONG, T.F. Pore and throat size distributions measured from synchrotron X-ray tomographic images of Fontainebleau sandstones. **Journal of Geophysical Research Solid Earth**, Hoboken, v. 105, n. B9, p. 21509–21527, 2000.

MUALEM, Y. A new model for predicting the hydraulic conductivity of unsaturated porous media. **Water Resources Research**, Hoboken, v. 12, n. 3, p. 513-522, 1976.

OH, S.; KIM, Y.K.; KIM, J.W. A Modified van Genuchten-Mualem Model of Hydraulic Conductivity in Korean Residual Soils. **Water Journal**, Basel, v. 7, p. 5487-5502, 2015.

OLLION, J.; COCHENNEC, J.; LOLL, F.; ESCUDÉ, C.; BOUDIER, T. TANGO: a generic tool for high-throughput 3D image analysis for studying nuclear organization. **Bioinformatics**, Oxford, v. 29, n. 14, p. 1840-1841, 2013.

PETERS, A.; DURNER, W. Simplified evaporation method for determining soil hydraulic properties. **Journal of Hydrology**, Amsterdam, v. 356, p. 147–162, 2008.

PINHEIRO, E.A.R.; DE JONG VAN LIER, Q.; METSELAAR, K. A matric flux potential approach to assess plant water availability in two climate zones in Brazil. **Vadose Zone Journal**, Madison, v. 16, n. 3, p. 1-10, 2017.

RENARD, P.; ALLARD, D. Connectivity metrics for subsurface flow and transport. **Advances in Water Resources**, Southampton, v. 51, p. 168-196, 2013.

SCHAAP, M.G.; LEIJ, F.J. Improved prediction of unsaturated hydraulic conductivity with the Mualem–van Genuchten model. **Soil Science Society of America Journal**, Madison, v. 64, p. 843–851, 2000.

SCHINDELIN, J.; ARGANDA-CARRERAS, I.; FRISE, E.; KAYNIG, V.; LONGAIR, M.; PIETZSCH, T.; PREIBISCH, S.; RUEDEN, C.; SAALFELD, S.; SCHMID, B.; TINEVEZ, J-Y.; WHITE, D. J.; HARTENSTEIN, V.; ELICEIR, K.; TOMANCAK, P.; CARDONA, A. Fiji: an open-source platform for biological-image analysis. **Nature Methods**, New York, v. 9, n. 7, p. 676-682, 2012.

SCHINDLER, U. Ein Schnellverfahren zur Messung der Wasserleitfähigkeit im teilgesättigten Boden an Stechzylinderproben. **Archiv für Acker- und Pflanzenbau und Bodenkunde**, Berlin, v. 24, p. 1–7, 1980.

SCHINDLER, U.; DURNER, W.; VON UNOLD, G.; MUELLER, L.; WIELAND, R. The evaporation method: Extending the measurement range of soil hydraulic properties using the air-entry pressure of the ceramic cup. **Journal of Plant Nutrition and Soil Science**, Weinheim, v. 173, p. 563–572, 2010.

SCHNEIDER, K.; IPPISCH, O.; ROTH, D.K. Novel evaporation experiment to determine soil hydraulic properties. **Hydrology and Earth System Sciences Journal**, Munich, v. 10, p. 817–827, 2006.

SCHLÜTER, S.; SHEPPARD, A.; BROWN, K.; WILDENSCHILD, D. Image processing of multiphase images obtained via X-ray microtomography: A review. **Water Resources Research**, Hoboken, v. 50, p. 3615–3639, 2014.

SCHLÜTER, S.; VOGEL, H.J. Analysis of Soil Structure Turnover with Garnet Particles and X-Ray Microtomography. **PLoS ONE**, San Francisco, v. 11, n. 7, p. 1-17, e0159948, 2016.

SCHUH, W.M.; CLINE, R.L. Effect of soil properties on unsaturated hydraulic conductivity pore-interaction factors. **Soil Science Society of America Journal**, Madison, v. 54, p. 1509–1519, 1990.

SIEGEL, S.; CASTELLAN JÚNIOR, N.J. **Estatística não-paramétrica para ciências do comportamento**. 2. ed. Porto Alegre: Artmed, 2006. 448 p.

ŠIMŮNEK, J.; WENDROTH, O.; VAN GENUCHTEN, M.T. Parameter estimation analysis of the evaporation method for determining soil hydraulic properties. **Soil Science Society of America Journal**, Madison, v. 62, p. 894-905, 1998.

TORIWAKI, J.; YONEKURA, T. Euler number and connectivity indexes of a three dimensional digital picture. **Forma**, Tokyo, v. 17, p. 183–209, 2002.

VAN GENUCHTEN, M. T. A closed-form equation for predicting the hydraulic conductivity of unsaturated soils. **Soil Science Society of America Journal**, Madison, v. 44, p. 892-898, 1980.

VAN GENUCHTEN, M.T.; LEIJ, F.J.; YATES, S.R. **The RETC code for quantifying the hydraulic functions of unsaturated soils**. Riverside, CA: USDA, U.S. Salinity Laboratory, 1991. (Document EPA/600/2-91/065).

VEREecken, H.; WEYNANTS, M.; JAVAUX, M.; PACHEPSKY, Y.; SCHAAP, M.G.; VAN GENUCHTEN, M.T. Using pedotransfer functions to estimate the van Genuchten–Mualem soil Hydraulic properties: A Review. **Vadose Zone Journal**, Madison, v. 9, p. 795–820, 2010.

VOGEL, H.J. Morphological determination of pore connectivity as a function of pore size using serial sections. **European Journal of Soil Science**, Oxford, v. 48, n. 3, p. 365–377, 1997.

VOGEL, H.J. A numerical experiment on pore size, pore connectivity, water retention, permeability, and solute transport using network models. **European Journal of Soil Science**, Oxford, v. 51, p. 99-105, 2000.

VOGEL, H.J.; ROTH, K. Quantitative morphology and network representation of soil pore structure. **Advances in Water Resources**, Southampton, v. 24, n. 3, p. 233–242, 2001.

VOGEL, H.J.; WELLER, U.; SCHLÜTER, S. Quantification of soil structure based on Minkowski functions. **Computers & Geosciences**, Oxford, v. 36, n. 10, p. 1236–1245, 2010.

WILDENSCHILD, D.; SHEPPARD, A. P. X-ray imaging and analysis techniques for quantifying pore-scale structure and processes in subsurface porous medium systems. **Advances in Water Resources**, Southampton, v. 51, p. 217–246, 2013.

WIND, G.P. Capillary conductivity data estimated by a simple method. In: RIJTEMA, R.E.; WASSINK H. (Ed.). **Water in the Unsaturated Zone**. Wageningen: IASH, 1968. v. 1, p. 181–191.

YATES, S.R.; VAN GENUCHTEN, M.TH.; WARRICK, A.W.; LEIJ, F.J. Analysis of measured, predicted, and estimated hydraulic conductivity using the RETC computer program. **Soil Science Society of America Journal**, Madison, v. 56, p. 347–354, 1992.

### 3 FUNCTIONAL EVALUATION OF SOIL HYDRAULIC PARAMETERIZATION IN SOME TROPICAL SOILS

#### Abstract

Soil hydraulic properties (SHP) are needed to quantify water balance components in vadose zone hydrological models. Retention properties can be measured directly using field or laboratory methods, but determining unsaturated hydraulic conductivity is more troublesome and commonly it is predicted from retention data, introducing an empirical parameter related to tortuosity and connectivity. The value of this parameter is usually not determined, but, instead, a standard value is applied. We evaluated the sensitivity of the predictions of an agro-hydrological model to the tortuosity/connectivity parameter, applying its commonly used standard value or determining its value in laboratory evaporation experiments using wet-range tensiometers, dry-range tensiometers, or both wet- and dry-range tensiometers. Four tropical soils from Brazil were used for the analysis. Simulations with the agro-hydrological model were performed for some years with distinct rainfall characteristics.

**Keywords:** tortuosity factor, SWAP, soil hydraulic properties

#### 3.1 Introduction

Soil hydraulic property (SHP) functions, i.e. the hydraulic conductivity and water retention functions, are essentials for vadose zone hydrological modeling applied to predict agronomic and ecological processes. Such models are used to simulate the transport of water, solutes and heat in saturated and unsaturated soil zones. Richards's equation (RICHARDS, 1948) based models integrated with plant growth modules can predict relative or absolute water-limited crop yield (DROOGERS et al., 2004; MO et al., 2005; DE JONG VAN LIER; WENDROTH; VAN DAM, 2015), water use efficiency, nutrient transport (WOLF et al., 2003; PINTO et al., 2017), irrigation management (UTSET et al., 2004; RALLO et al., 2012), and crop water availability (VAN WART; GRASSINI; CASMAN, 2013; IDEN; PETERS; DURNER, 2015; PINHEIRO; VAN LIER; METSELAAR, 2017), among other processes.

Whereas retention properties can be measured directly using relatively simple field or laboratory methods, determining hydraulic conductivity for unsaturated conditions is much more troublesome and commonly it is predicted from retention data using pore size models or statistical models. These models predict the hydraulic conductivity by integration of elementary pore domains, represented by a range of pore radii, e.g. the models of Childs and Collis-George

(1950), Burdine (1953) and Mualem (1976). To deal with the unknown pore space tortuosity and connectivity, an empirical parameter is introduced in these models.

In the Mualem (1976) hydraulic conductivity model, based on the capillary bundle theory, a parameter  $l$  was introduced to account for eccentricity of the flow path. The value of  $l = 0.5$  was obtained by Mualem (1976) using a data set of 45 soil samples. The physical meaning of  $l$  is unclear and it may be considered as an integral of all model uncertainties together (VOGEL, 2000).

Computed water balances are very sensitive to soil hydraulic parameters and therefore their accurate determination is essential to model hydrological processes (JOHRAR et al., 2004). Vereecken et al. (1992) showed that the uncertainty in hydraulic parameters results in a considerable variation of simulated soil moisture supply capacity and of the downward flux below the root zone.

In comprehensive analyses of soil-plant-atmosphere relations involving agro-hydrological simulations, models are parameterized and calibrated to simulate involved processes under specific climate, soil and plant scenarios, which may be based on present data or refer to expected or otherwise possible scenarios. Generally, models are projected to provide fair pictures of the behavior of the studied systems under likely scenarios, though, the reliability of simulations depends on model parameterization. Soil properties play a very important role in agro-hydrological simulations, especially because SHP determine all water fluxes, those towards the root system (driving plant growth), drainage and evaporation rate.

Even when simple soil-water relations approaches are used like the plant-available water calculated based on two water contents (field capacity and permanent wilting point), although commonly assumed to be related only to retention properties, in a more detailed process-based analysis those two water contents are determined by both water retention and pore connectivity viz. hydraulic conductivity (TAWARAKAVI; ŠIMŮNEK; SCHAAP, 2010; DE JONG VAN LIER; WENDROTH, 2016; ASSOULINE; OR, 2014).

Several methods of estimating SHP are currently available, however, most of them yield incomplete information, focusing only on water retention characteristics and pore size distribution, lacking information on pore arrangement and connectivity. Most of the agro-hydrological simulations are run with water retention data only, which probably underrepresents the process-based behavior of soil-plant-atmosphere systems. Regarding water retention, simpler indirect methods have been implemented, for instance, pedotransfer functions, which are predictive equations that relate more easily measurable general soil data to water retention and hydraulic parameters (BOUMA; VAN LANEN, 1987; BOUMA, 1989;

VAN DEN BERG et al., 1997). However, pedotransfer functions, besides of being subject to statistical errors, require a reliable and large dataset, and are mostly applied to soil water retention.

Analyzing evaporation experiment data using inverse solution methods stands as a powerful tool to characterize SHP for a large range of soil water contents (ŠIMŮNEK; WENDROTH; VAN GENUCHTEN, 1998; PINHEIRO; VAN LIER; METSELAAR, 2017). In this study, we assessed soil hydraulic properties from evaporation experiments for different pressure head ranges. The tortuosity factor  $l$  was fitted using water retention curves determined in the traditional pressure chamber desorption method. In order to analyze the adequacy of the parameterized SHP in predicting soil hydraulic processes and to pinpoint their effect on agro-hydrological simulations, a functional evaluation was performed for years with distinct rainfall characteristics under climatic conditions of a southeast Brazilian climate.

## **3.2 Material and Methods**

### **3.2.1 Soil sampling**

Undisturbed and disturbed soil samples were collected in four soils from distinct soil classes (Rhodic Ferralsol, Rhodic Lixisol, Xanthic Ferrasol and Rhodic Nitossol) located in São Paulo State, Brazil. Particle size distribution, bulk and particle density from the sampled soils are shown in Table 1. Both soils were sampled in their surface horizon, between the depths of 0.1 and 0.3 m. Two different sizes of undisturbed samples were collected: larger samples in PVC rings (75 mm diameter and 75 mm height) for subsequent use in the wet-range evaporation experiments, and smaller samples in aluminum rings (50 mm diameter and 30 mm height) to be used in the traditional desorption experiments and for the measurement of saturated hydraulic conductivity ( $K_s$ ) using a constant head permeameter. Disturbed soil material was used in dry-range evaporation experiments and for the determination of particle density and particle-size distribution.

Table 3.1 – Bulk density ( $D_b$ ), particle density ( $D_p$ ), particle size distribution and geographical location of the four sampled soils

Great Soil Group according to IUSS (2015)	$D_b$	$D_p$	Total Porosity	Particle size distribution			Geographical Location	
				Sand	Silt	Clay	Latitude	Longitude
	----kg m <sup>-3</sup> ----		m <sup>3</sup> m <sup>-3</sup>	-----kg kg <sup>-1</sup> -----				
Rhodic Ferralsol	1,506	2,577	0.416	0.603	0.071	0.326	-23° 06'	-46° 56'
Rhodic Lixisol	1,336	2,548	0.476	0.678	0.076	0.246	-23° 06'	-46° 55'
Xanthic Ferralsol	1,851	2,590	0.286	0.754	0.024	0.222	-22° 42'	-47° 37'
Rhodic Nitosol	1,547	2,822	0.452	0.346	0.253	0.401	-22° 42'	-47° 37'

### 3.2.2 Experiments

Three protocols of soil hydraulic parameterization were used: the traditional desorption method yielding retention data, and wet-range evaporation and dry-range evaporation methods, yielding both retention and hydraulic conductivity data.

The traditional desorption method, here identified as *RC*, followed the conventional procedure which consisted of measuring soil water content in the smaller samples after desorption at specific tensions. Tensions from -0.1 to -0.6 m were applied using a tension Table and for higher tensions (-1 to -150 m) a porous plate pressure chamber was used. The final water content of the soil sample was determined by comparing to oven-dry (105 °C) mass.

The wet-range evaporation experiments ( $EE_{wet}$ , measured pressure head between -1 and -10 m) were conducted using the larger undisturbed soil samples which were equipped with two Hyprop tensiometers (SCHINDLER et al., 2010) vertically inserted in the sample through drilled holes with centers at 25 and 50 mm vertical distance from the sample bottom. The methodology used to determine unsaturated hydraulic conductivity was the simplified evaporation method (SCHINDLER, 1980; PETERS; DURNER, 2008), a simplification of the Wind (1968) approach. The soil-water flux was determined by the measurement of water tension using the two tensiometer cells at different positions. Soil samples were saturated by capillarity and tensiometers inserted and the sample bottom was sealed. The assembly was placed on an auto-logging balance and the measurement cycle was started. The pressure head and sample mass were recorded at pre-determined times until the mass of the sample reached a constant value. At the end of the measurement, the final water

content of the soil sample was determined by oven drying at 105 °C. The mass and pressure head measurements were used for the calculation of the soil-water flux.

The dry-range evaporation experiments ( $EE_{dry}$ , measured pressure head range between -1.5 and -165 m) were carried out with disturbed soil samples. A polyvinyl chloride ring (0.1 m high and 0.1 m in diameter) was filled with air-dry and sieved soil material and slowly saturated with water from bottom to top by imbibition from a shallow layer of tap water. After that, the bottom was sealed and three polymer tensiometers were horizontally inserted in the sample through drilled holes with centers at 25, 50 and 75 mm vertical distance from the sample surface (VAN DER PLOEG et al., 2010; DURIGON et al., 2011; PINHEIRO; VAN LIER; METSELAAR, 2017). Then, the set of soil sample and tensiometers was placed on a precision balance. Measurements of ring sample weight and pressure heads were automatically logged every 10 min. The evaporation experiment was finished when the upper tensiometer reached a pressure head value below -165 m, which took in the order of 3 weeks. At the end of the measurement, the final water content of the soil sample was determined by oven drying at 105 °C.

### 3.2.3 Soil hydraulic parameterization (SHP)

Unsaturated SHP were assumed to be defined by  $K$ - $\theta$ - $h$  relations (equations 1 and 2) described by the Van Genuchten-Mualem model (VAN GENUCHTEN, 1980).

$$\Theta = \left[ 1 + |\alpha h|^n \right]^{1/n-1} \quad 3.1$$

$$K = K_s \Theta^l \left[ 1 - \left( 1 - \Theta^{n/(n-1)} \right)^{l-1/n} \right]^2 \quad 3.2$$

with  $\Theta = (\theta - \theta_r) / (\theta_s - \theta_r)$ ;  $\theta$ ,  $\theta_r$  and  $\theta_s$  are water content, residual water content and saturated water content ( $\text{m}^3 \text{m}^{-3}$ ), respectively;  $h$  is pressure head (m),  $K$  and  $K_s$  are hydraulic conductivity and saturated hydraulic conductivity, respectively ( $\text{m d}^{-1}$ ); and  $\alpha$  ( $\text{m}^{-1}$ ),  $n$  and  $l$  are fitting parameters.

Five sets of SHP were obtained for each soil:

1. Using the inverse solution obtained from evaporation experiment data from the wet range experiments ( $EE_{wet}$ )
2. Using the inverse solution obtained from evaporation experiment data from the dry range experiments ( $EE_{dry}$ )

3. Using the inverse solution obtained from evaporation experiment data from the wet and dry range experiments together ( $EE_{wet+dry}$ )
4. Using the retention data from tension Table / pressure chamber, measured  $K_s$  and  $l = 0.5$  ( $RC_{l=0.5}$ ),
5. Using the retention data from tension Table / pressure chamber, measured  $K_s$  and  $l$  fitted according to  $K$  values obtained in  $EE_{wet+dry}$  ( $RC_{l-fit}$ )

The first three sets ( $EE_{wet}$ ,  $EE_{dry}$ , and  $EE_{wet+dry}$ ) were obtained by an inverse one-dimensional solution using Hydrus-1D (ŠIMŮNEK; VAN GENUCHTEN; ŠEJNA, 2008). Hydrus-1D implements a Marquardt-Levenberg type parameter estimation technique for inverse optimization of soil hydraulic parameters (ŠIMŮNEK; VAN GENUCHTEN; ŠEJNA, 2012). The upper and lower water flow boundary conditions were set as atmospheric boundary condition and constant flux (zero), respectively. Surface evaporation flux for each time interval was calculated from observed mass difference over a time interval and used as a time variable boundary conditions. The following information from the experimental data was included into the objective function: (i) pressure heads measured at the two (for  $EE_{wet}$ ) or three (for  $EE_{dry}$ ) depths over time and (ii) the final soil water content. In order to achieve robust minimization, data associated to the different soil textural classes available in the soil hydraulic catalog of Hydrus-1D were used as starting values.

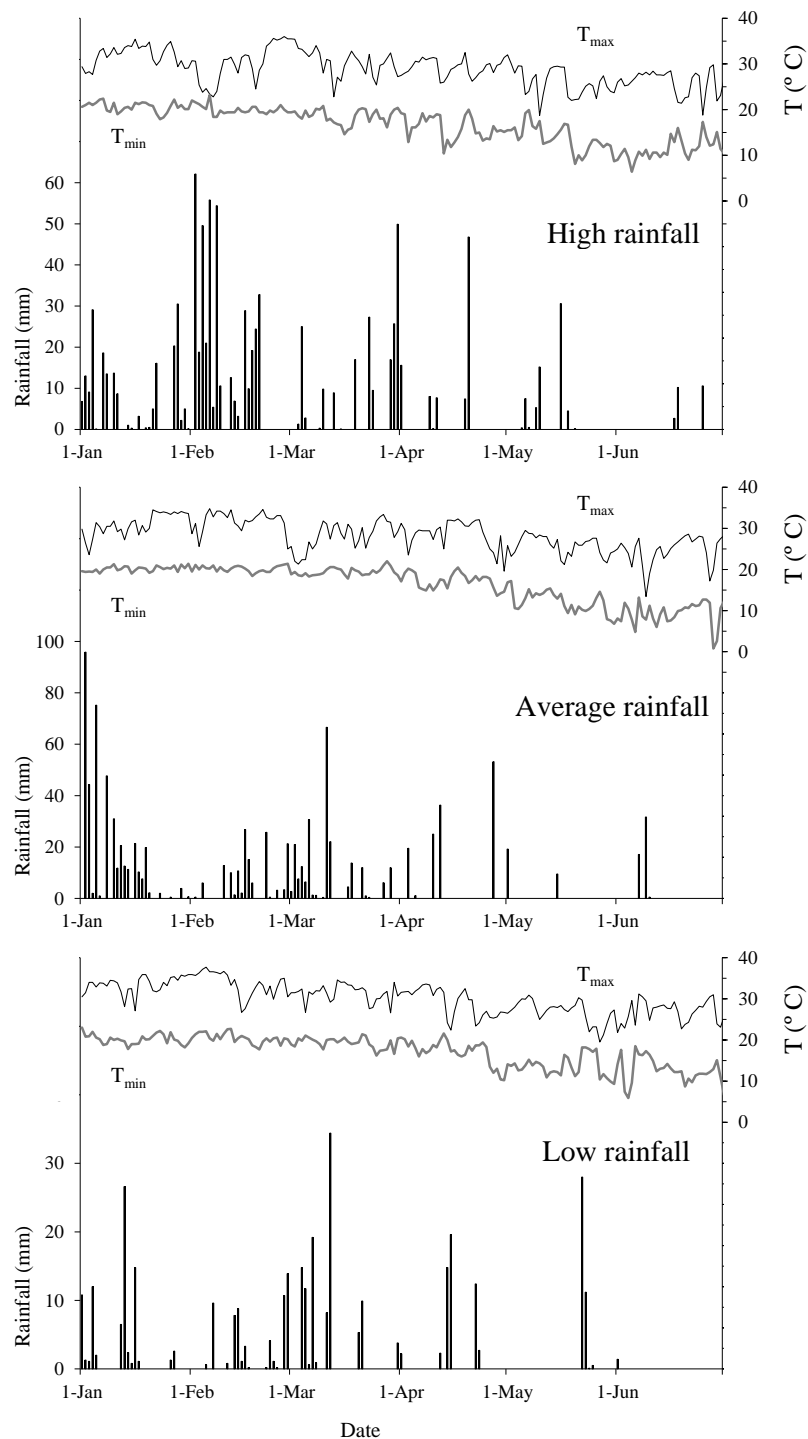
The water retention parameters SHP for the  $RC$  methods were obtained from retention data using the nonlinear least-squares optimization program RETC (VAN GENUCHTEN et al., 1991; YATES et al., 1992). For  $RC_{l=0.5}$ ,  $l$  was considered to be equal to 0.5 for all soils. For  $RC_{l-fit}$ , the value of  $l$  was optimized using the values of  $K$  observed in  $EE_{wet+dry}$ .

### 3.2.4 Agro-hydrological simulations

In order to functionally analyze the effect of the different protocols to achieve soil hydraulic parameterization using agro-hydrological simulations, we used the SWAP model (KROES et al., 2008) to simulate soils cropped with maize. Weather data were retrieved from the University of São Paulo weather station in Piracicaba, Brazil (22° 42' 30" S; 47° 38' 00" W, 546 m) for three distinct years in terms of rainfall: high rainfall (1995; 784 mm of rain during the crop growing season from February 1 to June 30), low rainfall (2014; 266 mm) and average rainfall (2011; 581 mm). The lower boundary condition for hydrological simulation was considered as free drainage, with a maximum rooting depth of 1 m.

Figure 3.1 shows the rainfall, maximum temperature and minimum temperature in Piracicaba for the three years from one month before seeding to the end of the simulated crop cycle.

Figure 3.1 – Rainfall, maximum temperature ( $T_{max}$ ) and minimum temperature ( $T_{min}$ ) observed at the Piracicaba weather station during the wet (1995), average (2011) and dry (2014) cropping seasons used in simulations



The SWAP model simulates water flow, solute transport and plant growth in a soil–water–atmosphere–plant environment. To calculate the water balance terms, the model employs the Richards equation with a root water extraction sink term:

$$\frac{\partial \theta}{\partial t} = \frac{\partial}{\partial z} \left[ K(h) \left( \frac{\partial h}{\partial z} + 1 \right) \right] - S(h) \quad 3.3$$

In this equation,  $t$  denotes time (d),  $z$  is the vertical coordinate taken as positive upwards (cm),  $K(h)$  is the hydraulic conductivity ( $\text{cm d}^{-1}$ ) and  $S(h)$  represents the water uptake by plant roots ( $\text{d}^{-1}$ ). Equation 3.3 is solved numerically describing the  $\theta$ – $h$ – $K$  relation by the Mualem–van Genuchten equations (MUALEM, 1976; VAN GENUCHTEN, 1980).

To estimate the sink term  $S(h)$ , the reduction function proposed by Feddes et al. (1976) and Feddes, Kowalik and Zaradny (1978) implemented in the SWAP model was used. It computes relative plant transpiration based on five threshold pressure heads (Table 3.2). Consequently, the prediction of crop water stress and crop transpiration under specific scenarios depends greatly on soil hydraulic parameterization, a poor parameterization being likely to bring about unreliable outcomes leading to possibly erroneous conclusions.

Table 3.2 – Threshold pressure head values of the Feddes, Kowalik and Zaradny (1978) reduction function for maize according to Taylor and Ashcroft (1972)

Parameter	Description	Value
$h_1$	No water extraction at higher pressure heads	0
$h_2$	$h$ below which optimum $RWU$ starts	-10
$h_{3h}$	$h$ below which $RWU$ reduction starts at high potential transpiration	-300
$h_{3l}$	$h$ below which $RWU$ reduction starts at low potential transpiration	-600
$h_4$	No water extraction at lower pressure heads	-3000

### 3.3 Results and Discussion

#### 3.3.1 Soil hydraulic parameterization

The five sets of SHP for each soil are shown in Table 3.3. Respective RMSE values correspond to each specific parameter fitting procedure. For  $RC_{l=0.5}$ , the parameter fitting was performed as function of  $\theta$  and the RMSE was calculated accordingly. For  $RC_{l-fit}$ , RMSE refers to the observed hydraulic conductivity data from the  $EE_{wet+dry}$  and to the predicted  $K$  for the

optimized  $l$ . The RMSE of  $EE_{dry}$  was calculated using  $h$  values; RMSE for  $EE_{wet+dry}$  was calculated related to  $K$ ; for  $EE_{wet}$ , RMSE was calculated using  $\log K$ .

When parameter fitting is based on the dry range alone, parameters at saturated conditions ( $\theta_s$  and  $K_s$ ) should be understood as mere fitting parameters and cannot be interpreted as if they were really measured at saturation. Extrapolation beyond the range of pressure heads measured during the evaporation experiment is associated with a high level of uncertainty (ŠIMŮNEK; WENDROTH; VAN GENUCHTEN, 1998).

Table 3.3 – Optimized van Genuchten-Mualem parameters (Eqs. 3.1 and 3.2) for the sampled soils, and RMSE values

Parameterization	$\theta_s$ ( $\text{m}^3 \text{m}^{-3}$ )	$\theta_r$ ( $\text{m}^3 \text{m}^{-3}$ )	$\alpha$ ( $\text{m}^{-1}$ )	$n$	$l$	$K_s$ ( $\text{m d}^{-1}$ )	RMSE
Rhodic Ferralsol							
$RC_{l=0.5}$	0.37	0.16	28.79	1.25	0.50	2.85	0.055 ( $\theta$ )
$RC_{l-fit}$	0.37	0.16	28.79	1.25	-2.18	2.85	7.685 ( $\log K$ )
$EE_{wet}$	0.30	0.16	7.70	1.50	0.00	6.47	0.068 ( $\log K$ )
$EE_{dry}$	0.31	0.16	0.64	1.16	-1.00	0.006	0.047 ( $h, \text{m}$ )
$EE_{wet+dry}$	0.30	0.22	17.58	1.20	0.00	27.51	0.623 ( $K, \text{m d}^{-1}$ )
Rhodic Lixisol							
$RC_{l=0.5}$	0.43	0.09	11.20	1.22	0.50	3.15	0.021 ( $\theta$ )
$RC_{l-fit}$	0.43	0.09	11.20	1.22	-1.42	3.15	6.911 ( $\log K$ )
$EE_{wet}$	0.40	0.09	13.22	1.51	0.00	3.10	0.061 ( $\log K$ )
$EE_{dry}$	0.22	0.07	0.003	1.20	4.36	0.15	0.03 ( $h, \text{m}$ )
$EE_{wet+dry}$	0.40	0.00	94.26	1.10	-4.05	75.00	0.293 ( $K, \text{m d}^{-1}$ )
Xanthic Ferrasol							
$RC_{l=0.5}$	0.28	0.10	2.09	1.37	0.50	0.03	0.008 ( $\theta$ )
$RC_{l-fit}$	0.28	0.10	2.09	1.37	-1.1	0.03	5.698 ( $\log K$ )
$EE_{wet}$	0.28	0.09	3.16	1.88	-0.87	0.26	0.099 ( $\log K$ )
$EE_{dry}$	0.24	0.18	0.003	1.08	0.00	0.003	0.00 ( $h, \text{m}$ )
$EE_{wet+dry}$	0.28	0.19	6.97	4.28	-1.84	21.18	0.05 ( $K, \text{m d}^{-1}$ )
Rhodic Nitossol							
$RC_{l=0.5}$	0.49	0.00	8.95	1.09	0.50	0.62	0.013 ( $\theta$ )
$RC_{l-fit}$	0.49	0.00	8.95	1.09	-7.10	0.62	6.184 ( $\log K$ )
$EE_{wet}$	0.37	0.10	5.92	1.19	-0.56	4.20	0.066 ( $\log K$ )
$EE_{dry}$	0.29	0.13	0.44	1.12	0.00	0.25	0.03 ( $h, \text{m}$ )
$EE_{wet+dry}$	0.37	0.21	7.64	1.32	-1.31	2.53	0.018 ( $K, \text{m d}^{-1}$ )

Figure 3.2 shows pressure head ( $h$ ) as function of volumetric water content ( $\theta$ ) for the parameterization methods. Retention curve parameters for  $RC_{l=0.5}$  and  $RC_{l-fit}$  were obtained from the same procedure and are identified in this Figure by  $RC$ . The fitting process in the  $EE_{wet+dry}$  parameterization fitted the parameter values between  $EE_{wet}$  and  $EE_{dry}$  values, i.e.,  $\theta_s EE_{wet+dry} \leq \theta_s EE_{wet}$  and  $\theta_r EE_{wet+dry} \geq \theta_r EE_{dry}$ . The shape of the  $EE_{wet+dry}$  retention curve for the Xanthic Ferralsol (Figure 3.2) is a result of the high value of  $\theta_r$  obtained for  $EE_{dry}$  (Table 3.3).

The discontinuity observed in Figure 3.2 between curves from different parameterizations may be due to the use of disturbed ( $EE_{dry}$ ) and undisturbed ( $EE_{wet}$  and  $RC$ ) soil samples in the different experiments. The traditional pressure chamber desorption curve  $RC$  tends to overestimate soil-water content close to saturation, whereas in the dry range curves come together. The fitted water retention model does not take into account adsorptive forces (LI; WARDLAW, 1986; LENORMAND, 1990; NIMMO, 1991, PETERS, 2013), it only accounts for capillary water retention, and according to Vereecken et al. (2010) this may lead to some undesirable drawbacks. Theoretically, the soil-water retention curve is measured under equilibrium conditions; however, practically, when measuring the soil-water retention curve e.g., using the porous plate pressure method, as the soil becomes drier, it deviates further from equilibrium (HUNT; SKINNER, 2005), this may be due to the lack of equilibrium at relatively high tensions which correspond to very low hydraulic conductivity, not providing equilibrium conditions.

Soil hydraulic conductivity is affected not only by soil pore size distribution (information contained in the retention curve), but also by pore continuity and tortuosity, which determine the flow path. The inclusion of parameter  $l$  in Equation , supposed to account for the correlation between pores and the flow path tortuosity, enhances the agreement between theoretical and experimental curves (MUALEM, 1976). For that reason, the use of a fixed value for  $l$ , like 0.5 as found for the Mualem (1976) data set, causes a mismatch in many soils and is likely to increase the uncertainty in hydrological simulations. According to Pachepsky (1990), the assumed constant value of  $l = 0.5$  is in disagreement with the fact that the tortuosity factor strongly depends on soil structure and texture in addition to its dependence on soil moisture content. Assouline and Or (2013) found that the value of the  $l$  (Equation 3.2) depends on the specific soil-fluid properties and varies considerably for different soils.

Figure 3.2 – Volumetric water content as function of soil matric potential for each soil; dots represent measured values and lines are fits.

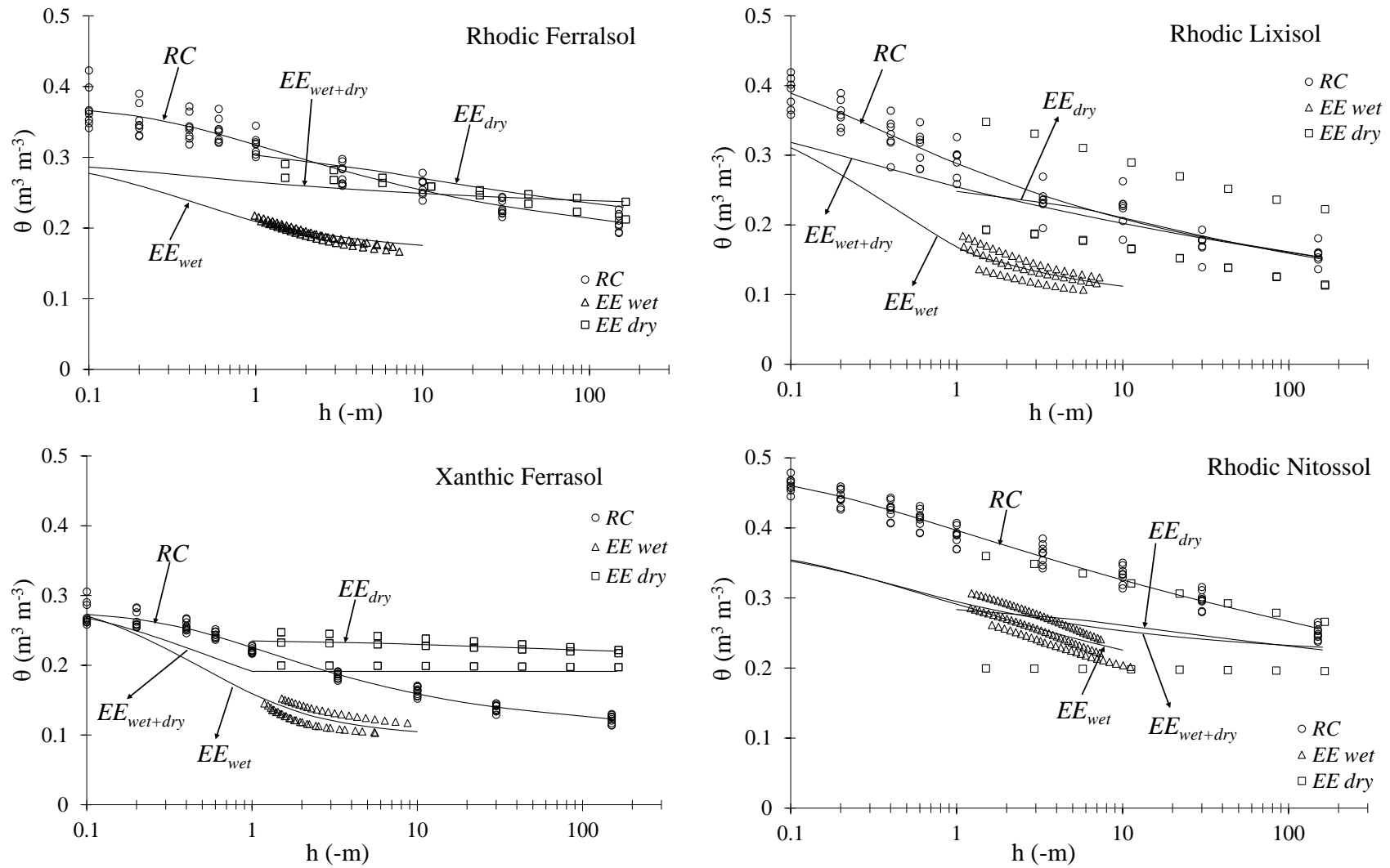
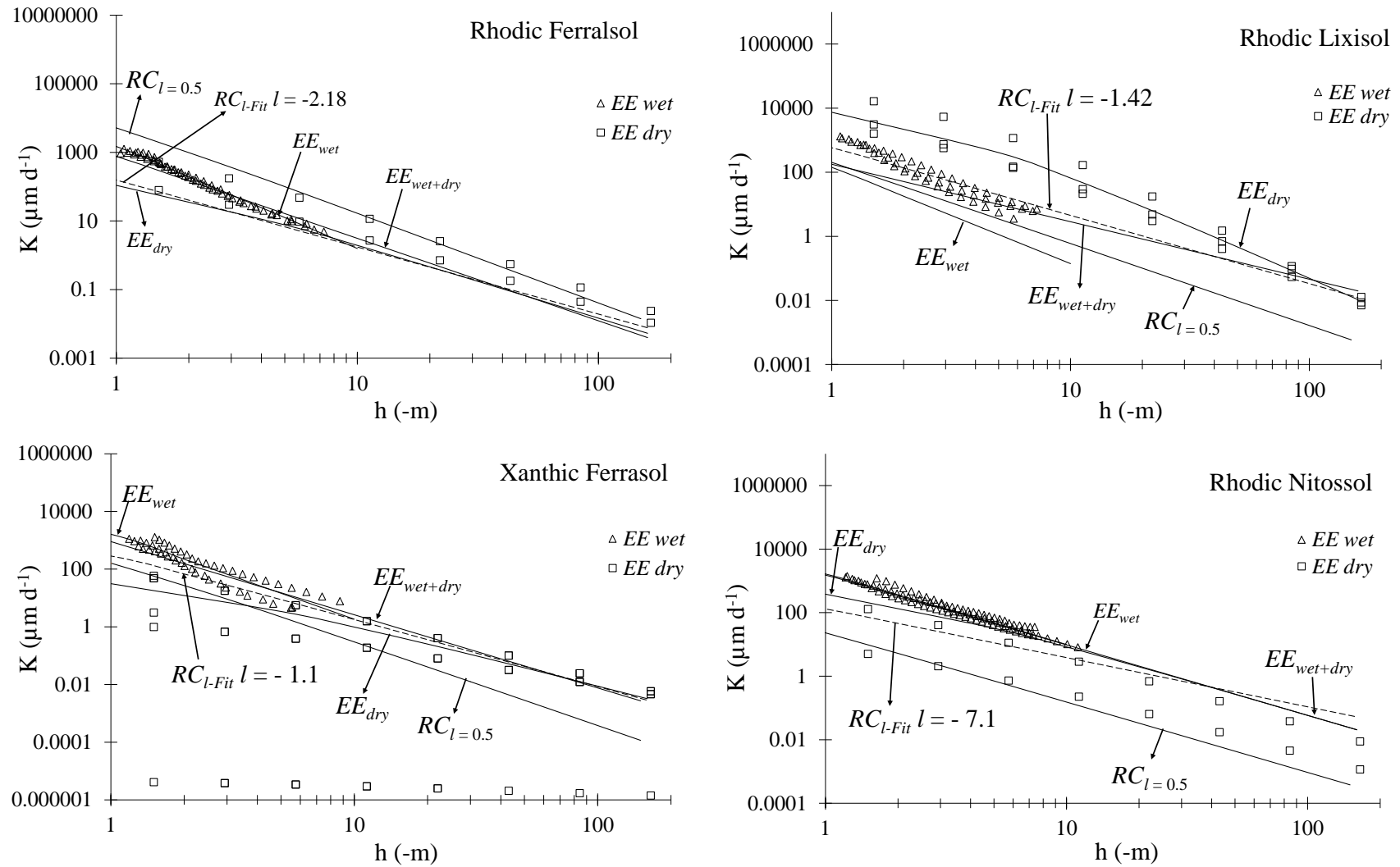


Figure 3.3 – Unsaturated hydraulic conductivity as function of soil matric potential; dots represent measured values and lines are fits



Observed values of the  $l$  parameter in our soils ranged from around -7 to +4 (Table 3.3). Negative values for  $l$  are often reported (SCHUH; CLINE, 1990; KAVEH; VAN GENUCHTEN, 1992; YATES et al., 1992; KOSUGI, 1999; SCHAAP; LEIJ, 2000; OH; KIM; KIM, 2015; PINHEIRO; VAN LIER; METSELAAR, 2017). Schaap and Leij (2000) found  $l = -1$ , as optimal value that minimizes root mean square error, on 235 soil samples on all texture range. Leij, Russell and Lesch (1997) obtained a mean value of  $l = -0.72$  when 401 pairs of water retention and unsaturated hydraulic conductivity data were considered. A negative value of  $l$  implies that the connectivity of water-filled pores increases with decreasing soil moisture content, which intuitively does not seem realistic (VEREECKEN et al., 2010). Therefore, some authors (HOFFMANN-RIEM; VAN GENUCHTEN; FLÜHLER, 1999; SCHAAP; LEIJ, 2000) suggest that  $l$  should be treated merely as an empirical parameter without physical meaning.

### 3.3.2 Agro-hydrological simulations

In addition to the numerical interpretation of parameter values, a functional interpretation will reveal the effect of parameter differences on soil processes as simulated by a hydrological model. Employing Richards equation-based models with a detailed description of soil-root zone processes allows to evaluate how different soil hydraulic parameterizations may impact model predictions of key processes in the soil-plant-atmosphere system.

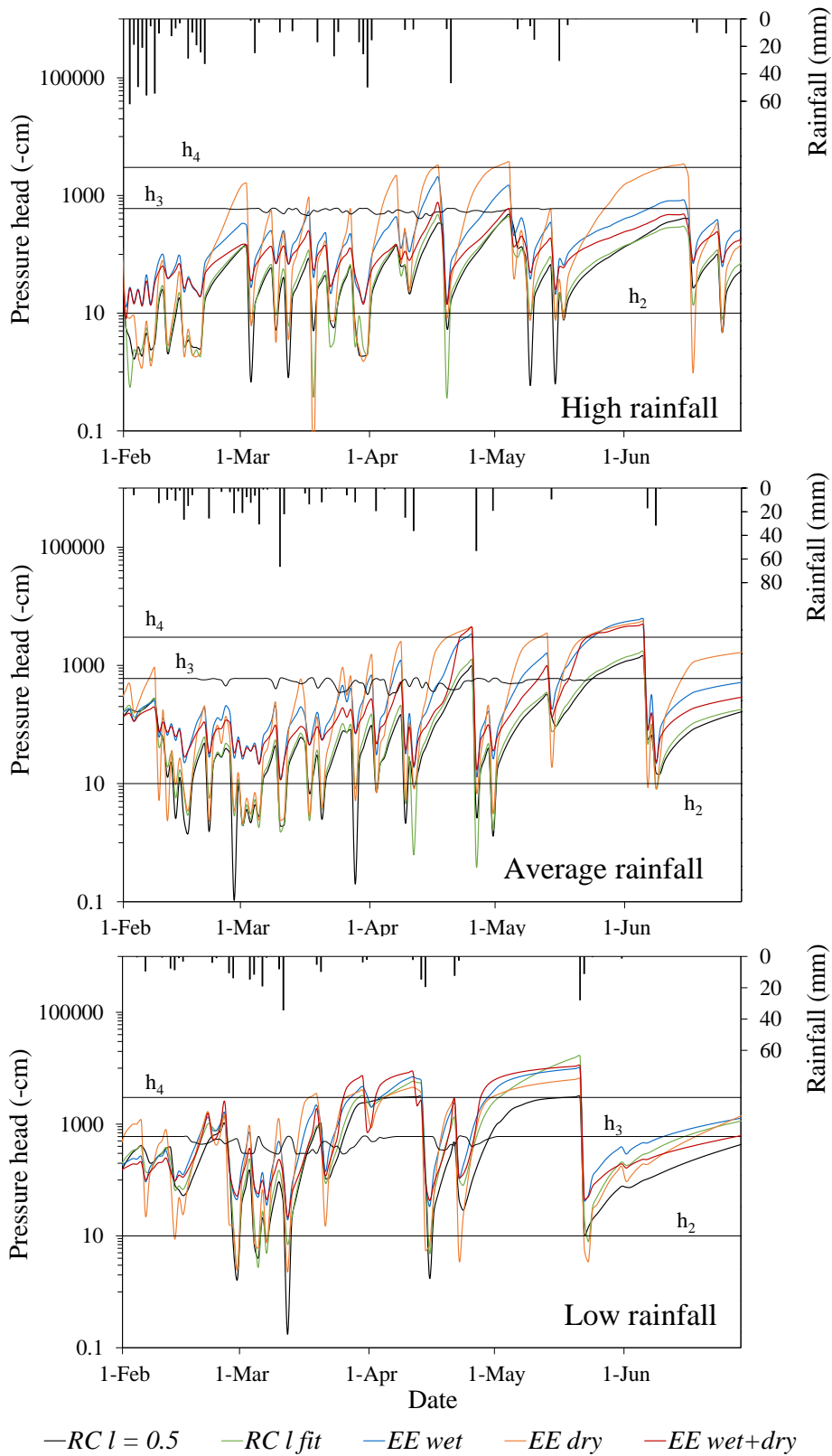
The simulated pressure head values at 10 cm depth during the maize crop cycle using the different set of SHP (Figure 3.4) show the stress occurrence by drought or water excess for the Rhodic Nitossol at the three rainfall scenarios. Figure 3.5 shows the same data for the average rainfall year in the four studied soils. The threshold pressure head that defines the onset of stress is based on the Feddes parameters compiled by Taylor and Ashcroft (1972) for the maize crop (Table 3.2). Pressure head values between thresholds  $h_2$  and  $h_3$  represent the optimum range for crop growth with absence of water stress.

In general, simulations using SHP from  $RC$  and  $RC_{l=0.5}$  predicted very short stress periods, while the other methods produced more restrictive scenarios. For the dry year, SHP obtained from the retention curve (with and without  $l$  fitting) and especially from  $EE_{dry}$ , simulated stress by water excess.

In every period in which there is accumulation of rainfall and/or intense rainfall event,  $EE_{dry}$ ,  $RC_{l=0.5}$  and  $RC_{l-fit}$  simulates an anoxic stress ( $h < h_2$ ), only at the Rhodic Lixisol (Figure 3.5)  $h$  decrease below  $h_2$  also for the  $EE_{wet+dry}$  parameterization. The low soil hydraulic

conductivity at high potentials presented by those parametrizations (Figure 3.3), which allows that occurs a slower water redistribution in the soil, along with soil already in wet condition, in the cases of accumulated rainfall, which causes the soil to remain with its water volumetric content close to saturation, providing the anoxic stress. Thus, the anoxic stress is sensible to values of  $K_s$ . In the case of Rhodic Lixisol for  $EE_{wet+dry}$  parameterization, besides a high value of  $K_s$ ,  $EE_{wet+dry}$  retention curve and hydraulic conductivity curve present low inclination, which causes low reduction of water volumetric content with increase of pressure.

Figure 3.4 – Pressure head simulated at 10 cm depth for the Rhodic Nitossol during the wet, average and dry year. Horizontal lines represent the Feddes threshold pressure heads  $h_2$ ,  $h_3$  and  $h_4$



Drought stress ( $h < h_3$ ) is simulated more frequently for soils with a low  $d\theta/dh$  in the dry part. When these soils approach dry conditions, a small reduction of the volumetric water content leads to a strong decrease in the potential. For the Rhodic Lixisol, Xanthic Ferralsol and Rhodic Nitosol,  $EE_{dry}$  and  $EE_{wet}$  simulate higher drought stress (Figure 3.5); while in Rhodic Ferralsol,  $EE_{wet+dry}$  is the parametrization that simulates the highest drought stress. Figure 3.2 shows the low inclination of the retention curve for the mentioned parameterizations that simulate drought stress and the respective soils. Values of  $h$  above  $h_4$  are also associated with a low inclination of the retention curve and occurs especially when atmospheric demand is high, more often during the dry year (Figure 3.4).

$RC_{l=0.5}$  and  $RC_{l-fit}$  at optimal conditions ( $h_2 \leq h \leq h_3$ ) have a similar behavior, however,  $RC_{l-fit}$  simulates higher pressure heads, due to its higher hydraulic conductivity, caused by the negative value of tortuosity factor. Under the same optimal condition for the Xanthic Ferralsol, simulated values of  $h$  are very similar for both  $RC_{l=0.5}$  and  $RC_{l-fit}$  ( $l = -1.1$ ). When  $h > h_2$ , their behavior becomes different.

$RC_{l=0.5}$ ,  $RC_{l-fit}$  and  $EE_{dry}$ , especially, simulated stresses by water excess at high and average rainfall, causing a drop in the simulated relative crop yield (Figure 3.6).  $EE_{wet}$  did not simulate stress by water excess for any year, not even for the wet year. Apparently, parametrization of only the dry part did not allow a proper simulation of near-saturated conditions, not resulting in excess water stress as simulated by  $EE_{wet}$ .

Simulations with  $EE_{dry}$  yielded different results than  $EE_{wet}$  and  $EE_{wet+dry}$ , especially for the wet and average year; thus, we can conclude that parameterization only for the dry-range is not adequate for simulations when wet condition are dominating. Figure 3.5 highlights this condition for the Rhodic Lixisol and Xanthic Ferrasol during the average year, where the  $EE_{dry}$  parameterization simulated very different conditions than other parameterizations, especially when compared to  $EE_{wet}$  and  $EE_{wet+dry}$ .

Hupet, Van Dam and VanClooster (2004) investigated the impact of within-field variability in the soil hydraulic properties on actual transpiration and dry matter yield for three different climate scenarios. They also evaluated sensitivity of the simulated actual transpiration and dry matter yield to soil hydraulic parameters, which increases with the dryness of the climate. Their simulation results showed very different results of the agro-hydrological simulations according to the climatic scenarios (wet, average and dry year). The sensitivity of the actual transpiration rate and the dry matter to the soil hydraulic parameters ( $\theta_s$ ,  $n$ ,  $\alpha$  and  $K_s$ ) was often very similar, being a direct consequence of conceptualizations in agro-hydrological models to reduce the daily potential gross  $CO_2$  assimilation rate.

Figure 3.5 – Simulated pressure head at 10 cm depth for the Rhodic Ferralsol, Rhodic Lixisol, Xanthic Ferrasol and Rhodic Nitossol during the average year

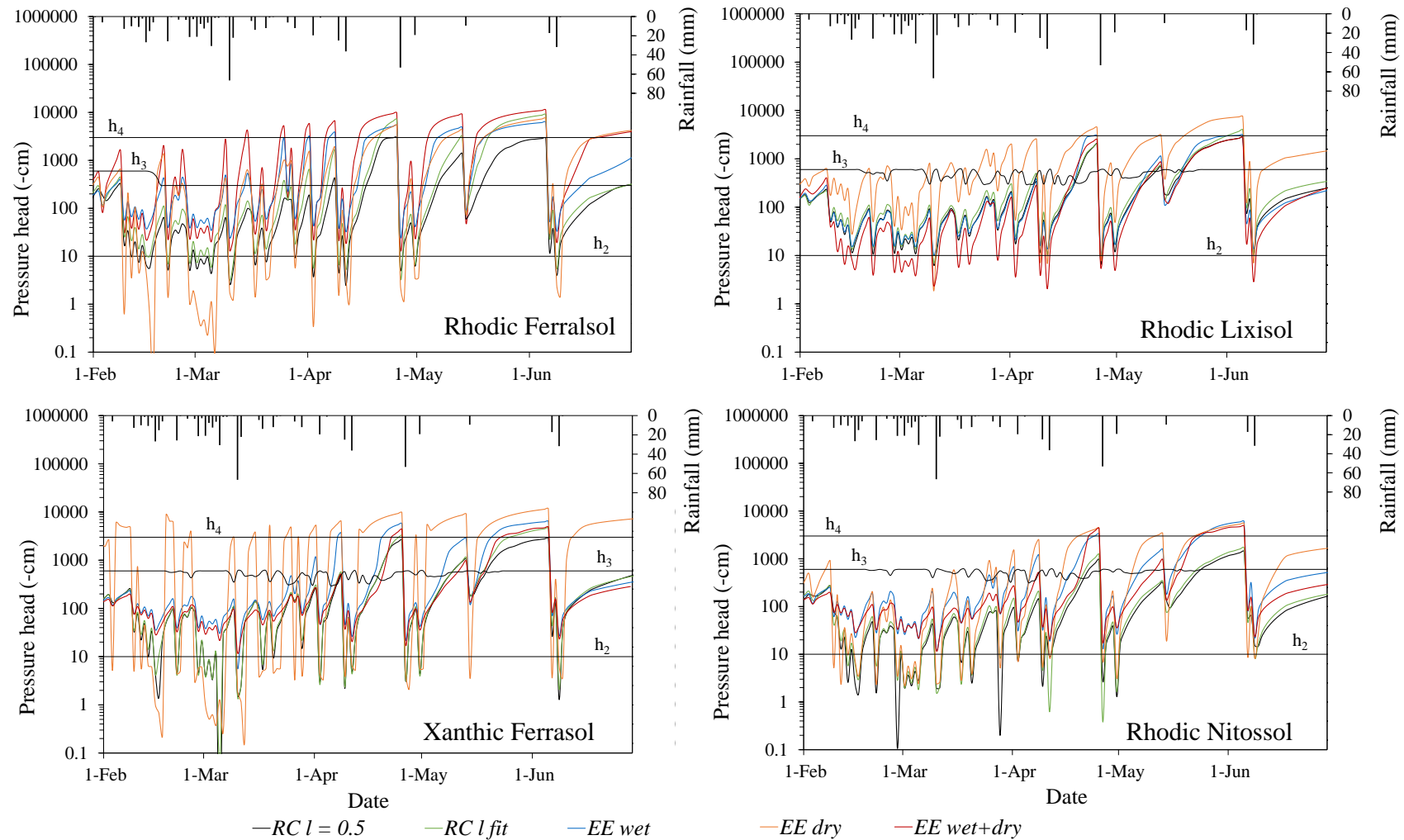


Figure 3.6 shows the relative yield, simulated by the SWAP model, for the particular case of the Rhodic Nitossol cropped with maize during the wet, average and dry year, while Figure 3.7 shows the maize relative yield simulated for the average year at the four soils studied, using the five soil hydraulic parameterizations. Relative yield was calculated by the quotient between potential yield and water-limited yield. Potential yield takes into account solar radiation, temperature, CO<sub>2</sub>, genetic potential of the plant, while the water-limited yield also takes into account water availability, which in our case, was simulated based on Feddes, Kowalik and Zaradny (1978) reduction function.

In well drained soils during periods with average and high rainfall, the relative yield is expected to reach values close to unity. In our simulations, only the SHP obtained from  $EE_{wet+dry}$  (the widest range of evaluated water contents) predicted relative yields close to the maximum. The simulation using SHP from  $EE_{wet}$  also reached values close to 1. For periods with rainfall supply, pressure heads of cropped soils hardly ever drop to very negative values, therefore, the SHP obtained from wet range experiments may be supposed to be able to yield good simulation results.

The simulations predicted low relative yield for the Xanthic Ferralsol for all five parameterizations (Figure 3.7), especially for  $EE_{dry}$ , due to the simulated stresses by drought and water excess (Figure 3.5). For all five parameterization methods this soil presented low values of  $\theta_s$ , due to the low total porosity ( $0.286 \text{ m}^3\text{m}^{-3}$ , Table 3.1), and high values of  $\theta_r$ , providing low soil water storage capacity. Besides that, the low inclination of the retention curve and the low hydraulic conductivity provided a stress-prone scenario.

The poor performance of simulation using SHP acquired from  $EE_{dry}$  is expected due to the lack of representativeness of SHP for wet conditions. The SHP from the retention curve with fitted tortuosity factor ( $l$ ) when compared to  $l = 0.5$ , resulted in relative yields closer to the simulation performed with  $EE_{wet+dry}$ . This shows that some constraints pointed by specific simulations in crop yield may be related to poor soil hydraulic parameterization rather than resource stress, e.g., water and energy. Yield predictions showed to be highly sensitive to soil hydraulic parameterization, even when this sensitivity does not show up strongly in predicted soil pressure head values.

Figure 3.6 – Predicted relative maize yield for the Rhodic Nitossol for the wet, average and dry year using the five different parameterizations

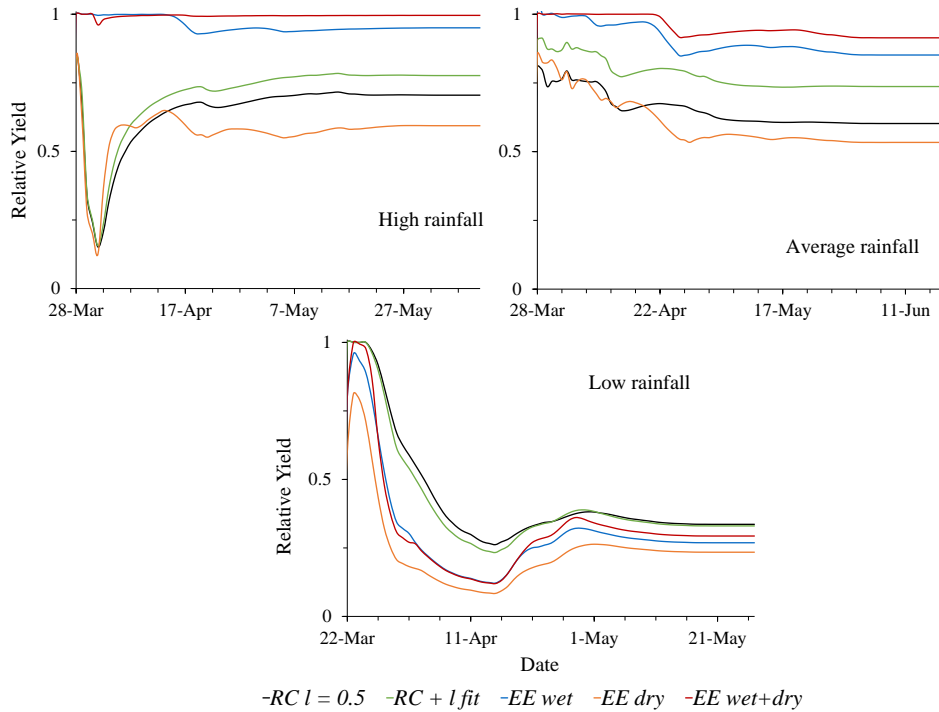
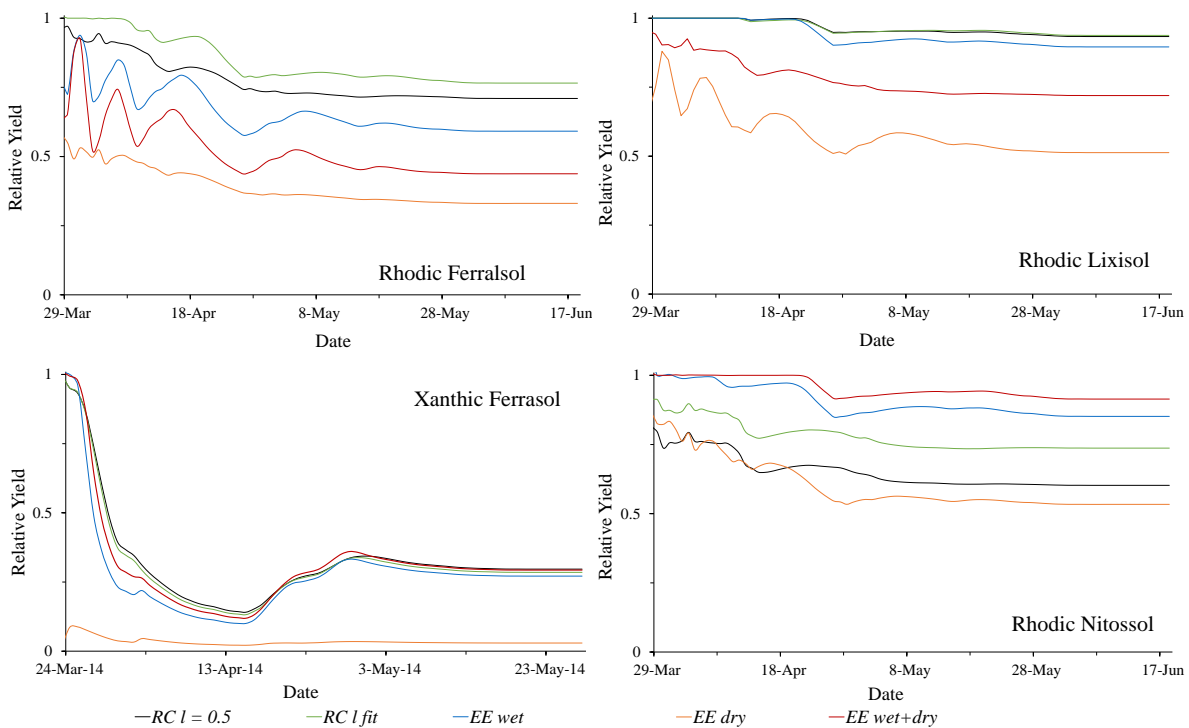


Figure 3.7 – Predicted relative maize yield for the Rhodic Ferralsol, Rhodic Lixisol, Xanthic Ferralsol and Rhodic Nitossol for the average year using the five different parameterizations



The use of fixed parameters or inappropriate parameterization may lead to large errors in the unsaturated hydraulic conductivity function (DURNER, 1994), impacting on predictions of unsaturated water flow in the vadose zone. None of current available measuring devices allows the measurement of the SHP over the entire range of soil water content (SCHELLE et al., 2013). The prediction of SHP from retention curve data with  $l$  optimized instead of a fixed value, as performed in this study, may be an interesting option, however, measurement techniques in which the natural soil structure is maintained and that provide records of soil-water content or pressure head from saturation to complete dryness over time, coupled with inverse solution (ŠIMŮNEK; WENDROTH; VAN GENUCHTEN, 1998), are essential for the understanding of unsaturated soil-water flow. As a recommendation, it is suggested that, where possible, perform measurements by the different methods on the same sample, ideally simultaneously.

### 3.4 Conclusions

1. The agro-hydrological simulations showed to be sensitive to the set of soil hydraulic parameters and to the range of pressure head for which they were determined. The existence of several uncertainties in the procedures of soil hydraulic parameterization restrain the extrapolation of soil hydraulic properties beyond the range of the  $K$ - $\theta$ - $h$  measured relation.
2. Although parameterization for the wet range can represent well the realm of pressure heads experienced by the most crop systems, soil hydraulic parameterization using a wider range of pressure head is necessary to represent soil-water-plant relations in dry lands, where low soil-water content is the general rule.
3. Comparing the simulation results using soil hydraulic properties from parameterization with retention data with a fixed value  $l = 0.5$  and with a fitted  $l$ , the latter behaved more similar to the methods using a measured  $K$ - $\theta$ - $h$  relation (parameterization for the wet and dry range and parameterization for the wet range).
4. The different methods to obtain the soil hydraulic properties were performed with different samples, some of them undisturbed and others sieved. Those factors are also embedded in the parameterizations results, and consequently, in simulations, and may have caused some of the observed differences.

## References

ASSOULINE, S.; OR, D. Conceptual and parametric representation of soil hydraulic properties: A review. **Vadose Zone Journal**, Madison, v. 12, p. 1-20, 2013.

ASSOULINE, S.; OR, D. The concept of field capacity revisited: Defining intrinsic static and dynamic criteria for soil internal drainage dynamics. **Water Resources Research**, Hoboken, v. 50, p. 4787–4802, 2014.

BOUMA, J. Using soil survey data for quantitative land evaluation. **Advances in Soil Science**, Oxford, v. 9, p. 177-213, 1989.

BOUMA, J.; VAN LANEN, H.A.J. Transfer functions and threshold values: From soil characteristics to land qualities. In: INTERNATIONAL WORKSHOP ON QUANTIFIED LAND EVALUATION PROCEDURES, 1987, Enschede, NE. **Proceedings...** Enschede, NE: ITC, 1987. p. 106-110. (Publication, 6).

BURDINE, N.T. Relative permeability calculations from pore size distribution data. **Transactions of Society for Mining, Metallurgy, and Exploration**, Littleton, CO, v. 198, p. 71–77, 1953.

CHILDS, E.C.; COLLIS-GEORGE, N. The permeability of porous materials. **Proceedings of the Royal Society of London. Series A: Mathematical and Physical Sciences**, London, v. 201, p. 392–405, 1950.

DE JONG VAN LIER, Q.; WENDROTH, O. Reexamination of the Field Capacity Concept in a Brazilian Oxisol. **Soil Science Society of America Journal**, Madison, v. 80, p. 264-274, 2016.

DE JONG VAN LIER, Q.; WENDROTH, O.; VAN DAM, J.C. Prediction of winter wheat yield with the SWAP model using pedotransfer functions: An evaluation of sensitivity, parameterization and prediction accuracy. **Agricultural Water Management**, Amsterdam, v. 154, p. 29–42, 2015.

DROOGERS, P.; VAN DAM, J.C.; HOOGEVEEN, J.; LOEVE, R. Adaptation strategies to climate change to sustain food security. In: AERTS, J.C.J.H.; DROOGERS, P. (Ed.). **Climate change in contrasting river basins**. London: CABI Publishers, 2004. p. 49–74.

DURIGON, A.; GOOREN, H.P.A.; VAN LIER, Q.J.; METSELAAR, K. Measuring hydraulic conductivity to wilting point using polymer tensiometers in an evaporation experiment. **Vadose Zone Journal**, Madison, v. 10, p. 741-746, 2011.

DURNER, W. Hydrological conductivity estimation with heterogeneous pore structure. **Water Resources Research**, Hoboken, v. 30, p. 211-223, 1994.

FEDDES, R.A.; Kowalik, P.J.; KOLINSKA-MALINKA, K.; ZARADNY, H. Simulation of field water uptake by plants using a soil water dependent root extraction function. **Journal of Hydrology**, Amsterdam, v. 31, p. 13–26, 1976.

FEDDES, R.A.; KOWALIK, P.J.; ZARADNY, H. **Simulation of field use and crop yield**. Wageningen, NE: Centre for Agricultural Publishing and Documentation, 1978. 189 p.

HOFFMANN-RIEM, H.; VAN GENUCHTEN, M.TH.; FLÜHLER, H. A general model of the hydraulic conductivity of unsaturated soils. In: INTERNATIONAL WORKSHOP ON CHARACTERIZATION AND MEASUREMENTS OF THE HYDRAULIC PROPERTIES OF UNSATURATED POROUS MEDIA, 1997, Riverside, CA. **Proceedings...** Riverside, CA: University of California, 1999. p. 31–42.

HUNT, A.G.; SKINNER, T.E. Hydraulic conductivity limited equilibration: effect on water retention characteristics. **Vadose Zone Journal**, Madison, v. 4, p. 145–150, 2005.

HUPET, F.; VAN DAM, J.C.; VANCLOOSTER, M. Impact of within-field variability in soil hydraulic properties on transpiration fluxes and crop yields: A numerical study. **Vadose Zone Journal**, Madison, v. 3, p. 1367–1379, 2004.

IDEN, S.C.; PETERS, A.; DURNER, W. Improving prediction of hydraulic conductivity by constraining capillary bundle models to a maximum pore size. **Advances in Water Resources**, Southampton, v. 85, p. 86–92, 2015.

IUSS WORKING GROUP WRB. **World Reference Base for Soil Resources 2014**: International soil classification system for naming soils and creating legends for soil maps. Rome: FAO, 2015. 203 p. (World Soil Resources Reports, 106).

JOHRAR, R.K.; VAN DAM, J.C.; BASTIAANSAN, W.G.M.; FEDDES, R.A. Calibration of effective soil hydraulic parameters of heterogeneous soil profiles. **Journal of Hydrology**, Amsterdam, v. 285, p. 233–247, 2004.

KAVEH, F.; VAN GENUCHTEN, M.Th. A further look at a new unsaturated hydraulic conductivity equation. **Iranian Journal of Agricultural Science**, Tehran, v. 23, p. 24–32, 1992.

KOSUGI, K. General model for unsaturated hydraulic conductivity for soils with lognormal pore-size distribution. **Soil Science Society of America Journal**, Madison, v. 63, p. 270–277, 1999.

KROES, J.G.; VAN DAM, J.C.; GROENENDIJK, P.; HENDRIKS, R.F.A.; JACOBS, C.M.J. **SWAP version 3.2**: Theory description and user manual. Wageningen, NE: Alterra, 2008. 255 p. (Altera Report, 1649).

LEIJ, F.J.; RUSSELL, W.B.; LESCH, S.M. Closed form expressions for water retention and conductivity data. **Groundwater**, Worthington, v. 35, p. 848–858, 1997.

LENORMAND, R. Liquids in porous media. **Journal of Physics: Condensed Matter**, Bristol, v. 2, SA79–SA88, 1990.

LI, Y.; WARDLAW, N.C. Mechanisms of nonwetting phase trapping during imbibition at slow rates. **Journal of Colloid and Interface Science**, New York, v. 109, p. 473–486, 1986.

MO, X.; LIU, S.; LIN, Z.; XU, Y.; XIANG, Y.; MCVICAR, T.R. Prediction of crop yield, water consumption and water use efficiency with a SVAT-crop growth model using remotely sensed data on the North China Plain. **Ecological Modelling**, Amsterdam, v. 183, n. 2, p. 301-322, 2005.

MUALEM, Y. A new model for predicting the hydraulic conductivity of unsaturated porous media. **Water Resources Research**, Hoboken, v. 12, n. 3, p. 513-522, 1976.

NIMMO, J.R. Comment on the treatment of residual water content in “A consistent set of parametric models for the two-phase flow of miscible fluid in the subsurface” by L. Luckner et al. **Water Resources Research**, Hoboken, v. 27, p. 661–662, 1991.

OH, S.; KIM, Y.K.; KIM, J.W. A Modified van Genuchten-Mualem Model of Hydraulic Conductivity in Korean Residual Soils. **Water Journal**, Basel, v. 7, p. 5487-5502, 2015.

PACHEPSKY, Y.A. **Mathematical models of physico-chemical processes in soil**. (In Russian). Moskow, Russia: Nauka, 1990. 188 p.

PETERS, A. Simple consistent models for water retention and hydraulic conductivity in the complete moisture range. **Water Resources Research**, Hoboken, v. 49, p. 6765-6780, 2013.

PETERS, A.; DURNER, W. Simplified evaporation method for determining soil hydraulic properties. **Journal of Hydrology**, Amsterdam, v. 356, 147-162, 2008.

PINHEIRO, E.A.R.; VAN LIER, Q.J.; METSELAAR, K. A Matric Flux Potential Approach to Assess Plant Water Availability in Two Climate Zones in Brazil. **Vadose Zone Journal**, Madison, v. 16, n. 3, p. 1-10, 2017.

PINTO, V.M.; BRUNO, I.P.; DE JONG VAN LIER, Q.; DOURADO-NETO, D.; REICHARDT, K. Environmental benefits of reducing N rates for coffee in the Cerrado. **Soil & Tillage Research**, Amsterdam, v. 166, p. 76-83, 2017.

RALLO, G.; AGNESE, C.; MINACAPILLI, M.; PROVENZANO, G. Comparison of SWAP and FAO Agro-Hydrological Models to Schedule Irrigation of Wine Grapes. **Journal of Irrigation and Drainage Engineering**, Reston, v. 138, n. 7, p. 581–591, 2012.

RICHARDS, L.A. Porous plate apparatus for measuring moisture retention and transmission by soils. **Soil Science**, Baltimore, v. 66, p. 105–110, 1948.

SCHAAP, M.G.; LEIJ, F.J. Improved prediction of unsaturated hydraulic conductivity with the Mualem–van Genuchten model. **Soil Science Society of America Journal**, Madison, v. 64, p. 843–851, 2000.

SCHELLE, H.; HEISE, L.; JÄNICKE, K.; DURNER, W. Water retention characteristics of soils over the whole moisture range: a comparison of laboratory methods. **European Journal of Soil Science**, Oxford, v. 64, p. 814–821, 2013.

SCHINDLER, U. Ein Schnellverfahren zur Messung der Wasserleitfähigkeit im teilgesättigten Boden an Stechzylinderproben. **Archiv für Acker- und Pflanzenbau und Bodenkunde**, Berlin, v. 24, p. 1–7, 1980.

SCHINDLER, U.; MÜLLER, L. Simplifying the evaporation method for quantifying soil hydraulic properties. **Journal of Plant Nutrition and Soil Science**, Weinheim, v. 169, p. 623-629, 2006

SCHINDLER, U.; DURNER, W.; VON UNOLD, G.; MUELLER, L.; WIELAND, R. The evaporation method: Extending the measurement range of soil hydraulic properties using the air-entry pressure of the ceramic cup. **Journal of Plant Nutrition and Soil Science**, Weinheim, v. 173, p. 563–572, 2010.

SCHUH, W.M.; CLINE, R.L. Effect of soil properties on unsaturated hydraulic conductivity pore-interaction factors. **Soil Science Society of America Journal**, Madison, v. 54, p. 1509–1519, 1990.

ŠIMŮNEK, J.; VAN GENUCHTEN, M.Th.; ŠEJNA, M. HYDRUS: Model use, calibration, and validation. **Transactions of the ASABE**, St. Joseph, v. 55, p. 1261–1274, 2012. doi:10.13031/2013.42239.

ŠIMŮNEK, J.; VAN GENUCHTEN, M.Th.; ŠEJNA, M. Development and applications of the HYDRUS and STANMOD software packages and related codes. **Vadose Zone Journal**, Madison, v. 7, p. 587–600, 2008. doi:10.2136/vzj2007.0077.

ŠIMŮNEK, J.; WENDROTH, O.; VAN GENUCHTEN, M.T. Parameter estimation analysis of the evaporation method for determining soil hydraulic properties. **Soil Science Society of America Journal**, Madison, v. 62, p. 894-905, 1998.

TAYLOR, S.A.; ASHCROFT, G.M. **Physical edaphology**. San Francisco, CA: Freeman, 1972. p. 434–435.

TAWARAKAVI, N.K.C.; ŠIMŮNEK, J.; SCHAAP, M.G. Can texture-based classification optimally classify soils with respect to soil hydraulics? **Water Resources Research**, Hoboken, v. 46, p. 1-11, W01501, 2010.

UTSET, A.; IMMA, F.; MARTINEZ-COB, A.; CAVERO, J. Comparing Penman-Monteith and Priestley-Taylor as reference evapotranspiration inputs for modeling maize water use under Mediterranean conditions. **Agricultural Water Management**, Amsterdam, v. 66, p. 205–219, 2004.

VAN DEN BERG, M.; KLAMT, E.; VANREEUWIJK, L.P.; SOMBROEK, W.G. Pedotransfer functions for the estimation of moisture retention characteristics of Ferralsols and related soils. **Geoderma**, Amsterdam, v. 78, p. 161-180, 1997.

VAN DER PLOEG, M.J.; GOOREN, H.P.A.; BAKKER, G.; HOOGENDAM, C.W.; HUISKES, C.; KOOPAL, L.K.; KRUIDHOF, H.; DE ROOIJ, G.H. Polymer tensiometers with ceramic cones: direct observations of matric pressures in drying soils. **Hydrology and Earth System Sciences Journal**, Munich, v. 14, p. 1787–1799, 2010.

VAN GENUCHTEN, M.T. A closed-form equation for predicting the hydraulic conductivity of unsaturated soils. **Soil Science Society of America Journal**, Madison, v. 44, p. 892-898, 1980.

VAN GENUCHTEN, M.T.; LEIJ, F.J.; YATES, S.R. **The RETC code for quantifying the hydraulic functions of unsaturated soils**. Riverside, CA: USDA, U.S. Salinity Laboratory, 1991. (Document EPA/600/2-91/065).

VAN WART, J.; GRASSINI, P.; CASMAN, K.G. Impact of derived global weather data on simulated crop yields. **Global Change Biology**, Oxford, v. 19, p. 3822–3834, 2013.

VEREECKEN, H.; DIELS, J.; VAN ORSHOVEN, J.; FEYEN, J.; BOUMA, J. Functional evaluation of pedotransfer functions for the estimation of soil hydraulic properties. **Soil Science Society of America Journal**, Madison, v. 56, p. 1371–1378, 1992.

VEREECKEN, H.; WEYNANTS, M.; JAVAUX, M.; PACHEPSKY, Y.; SCHAAP, M.G.; VAN GENUCHTEN, M.T. Using pedotransfer functions to estimate the van Genuchten–Mualem soil hydraulic properties: a review. **Vadose Zone Journal**, Madison, v. 9, n. 4, p. 795–820, 2010.

VOGEL, H.J. A numerical experiment on pore size, pore connectivity, water retention, permeability, and solute transport using network models. **European Journal of Soil Science**, Oxford, v. 51, p. 99–105, 2000.

WIND, G.P. Capillary conductivity data estimated by a simple method. In: RIJTEMA, R.E.; WASSINK H. (Ed.). **Water in the Unsaturated Zone**. Wageningen: IASH, 1968. v. 1, p. 181–191.

WOLF, J.; BEUSEN, A.H.W.; GROENENDIJK, P.; KROON, T.; RÖTTER, R.; VAN ZEIJTS, H. The integrated modeling system STONE for calculating emissions from agriculture in the Netherlands. **Environmental Modelling & Software**, Oxford, v. 18, p. 597–617, 2003.

YATES, S.R.; VAN GENUCHTEN, M.Th.; WARRICK, A.W.; LEIJ, F.J. Analysis of measured, predicted, and estimated hydraulic conductivity using the RETC computer program. **Soil Science Society of America Journal**, Madison, v. 56, p. 347–354, 1992.